Int. J. Heat Mass Transfer. Vol. 11, pp. 1491–1512. Pergamon Press 1968. Printed in Great Britain

THE GROWTH RATE OF VAPOUR BUBBLES IN SUPERHEATED PURE LIQUIDS AND BINARY MIXTURES

PART II: EXPERIMENTAL RESULTS

S. J. D. VAN STRALEN†

Heat Transfer Section, Technological University, Eindhoven, The Netherlands

(*Received* 5 *September* 1967)

Abstract—Growth rates of bubbles, generated at a moderate heat flux density in nucleate boiling on an electrically heated platinum wire immersed in water, and in water–methylethylketone ($x_0 = 4{\cdot}1 \times 10^{-2}$) and water–1-butanol ($x_0 = 1{\cdot}5 \times 10^{-2}$ and $x_0 = 6{\cdot}0 \times 10^{-2}$) mixtures, have been investigated. A high speed motion picture camera technique has been used. The experimental values of the growth constants $C_{1,p}$ and $C_{1,m}$ for ascending released bubbles are generally in quantitative agreement with theoretical predictions for free bubbles, e.g. the occurrence of a minimal $C_{1,m}$ at $x_0 = 1{\cdot}5 \times 10^{-2}$ for water–1-butanol. For the investigated water–methylethylketone mixture, a decreased $C_{1,m} = 0{\cdot}20\ C_{1,p}$ and a decreased $R_{1,m} = 0{\cdot}35\ R_{1,p}$ occur.

However, several bubbles show an unusual behaviour, i.e. higher or lower growth rates resulting from an increased or decreased distance, respectively, from their nearest neighbours. Sometimes bubbles have been observed, which oscillate both in shape and volume. In most cases, these vibrations are not originating from coalescence. The amplitude of the oscillations decreases due to viscous damping and ascending bubbles are gradually flattened. The frequency of the most important mode of vibration, the slowest fundamental harmonic, is in agreement with theory.

Some bubbles, generated in nucleate boiling and in film boiling of the azeotropic water–ethanol mixture, have been investigated. A hysteresis effect in the local liquid superheating has been observed.

1. INTRODUCTION

1.1. *General survey*

ALREADY in the thirties, Jakob *et al.* [1] were using motion pictures on steam bubbles, taken at a rate of approximately 500 frames per second (f.p.s.). Growth curves were obtained for some nonspherical bubbles, up to a departure radius $R_1 = 4 \times 10^{-3}$ m, and up to a radius $R = 6 \times 10^{-3}$ m after release. A comparison was made with the predictions following from the theoretical Bošnjaković–Jakob model, cf. Sections 1.1 to 1.3 of Part I [2].

Higher camera speeds (10^4–10^5 f.p.s.) are necessary, especially for the determination of the high initial growth rates of adhering bubbles as blurring occurs at low speeds. As a consequence, in all more recent investigations, high-speed camera techniques have been used to obtain more adequate information. The reader is referred to the original publications for a description of the experimental setup and for details concerning the photographic technique.

The growth rate of free bubbles in initially uniformly superheated water has been studied by Dergarabedian [3] at various degrees of superheating; the data are in quantitative agreement with the theoretical Forster–Zuber and Plesset–Zwick model, cf. equations (25) and (49) of Part I [2], i.e. $R(t) \sim \Delta\theta_0$, $R(t) \sim t^{\frac{1}{2}}$ and $C_{1,p} = 24 \times 10^{-4}$ m/s$^{\frac{1}{2}}$ degC.

Westwater and Santangelo [4, 5] studied the different regions of the boiling curve for methanol, boiling on a steam-heated copper tube (4000 f.p.s.). Westwater [6] determined

† Doctor of Physics, Principal Research Scientist.

growth rates in boiling pentane and observed vibrations of some bubbles.

Further research on bubble growth at atmospheric pressure in boiling binary mixtures includes experiments carried out by:

(i) Benjamin and Westwater [7] on free bubbles in ethyleneglycol–water at 4, 8 and 18 degC superheating. A minimum growth constant $C_{1,m}$ was found at approximately 5 wt % water. A maximum peak flux density $q_{w,max}$ had previously been observed by van Wijk, Vos and van Stralen [8], at nearly the same low concentration of the more volatile component, viz. at 2 wt % water. A scattering in the exponent n^* (0·40–0·80) of the time in the expression $R(t) \sim t^{n^*}$ was observed instead of the theoretical value of 0·50. This may be due to local temperature fluctuations and to local inhomogenities in the composition.

(ii) Van Wijk and van Stralen [9] on released bubbles generated in nucleate boiling of water–methylethylketone.

(iii) Van Stralen [10] on released bubbles in water–1-butanol.

(iv) Van Stralen [11] on adhering and released bubbles generated both in nucleate boiling and in film boiling of the azeotropic water–ethanol mixtures.

(v) Van Stralen [12] on adhering bubbles in nucleate boiling of water–methylethylketone and water–1-butanol.

(vi) Yatabe and Westwater [13] on free bubbles in water–ethanol and ethanol–isopropanol mixtures.

The bubble growth in pure liquids boiling at elevated pressures has been studied by:

(vii) Séméria [14] for adhering bubbles in water, boiling in the range from 5×10^{-3} —0·5 times the critical pressure. It is shown that the departure radius decreases rapidly with increasing pressure, in good agreement with van Stralen's "relaxation microlayer" theory [12] as the pressure $\sim \rho_2 \sim 1/C_{1,p} \sim 1/R_{1,p}$.

(viii) Wanninger [15] for adhering and ascending released bubbles in uniformly superheated pentane, in the range from 0·2–0·7 times the critical pressure. The bubble radius $R(t) \sim \Delta\theta_0$, $R(t) \sim t^{\frac{1}{2}}$ for adhering and for slowly ascending bubbles, and $R(t) \sim t$ after some time for released bubbles. The experimental ratio $(dR/dt)/\Delta\theta_0$, which is $\sim C_{1,p} \sim 1/\rho_2$ theoretically, decreased for increasing pressure.

Bubble growth and condensation rates in surface boiling of subcooled liquids have been investigated by Gunther [16] and by Ellion [17]. The present paper includes a description of the results of (ii–v).

1.2. *Scope of the present study*

The growth constant $C_{1,m}$ (x_0) of vapour bubbles is deduced here from experimental $R(t)$-curves for released bubbles for the binary systems water–methylethylketone and water–1-butanol. $C_{1,m}$, in combination with the liquid superheatings θ_0 and $\Delta\theta_0$, determines not only the growth rate of adhering and released bubbles generated in nucleate boiling, but also the bubble radius $R_1 = R(t_1)$ at departure and the bubble frequency [12]. The theory predicts the occurrence of a minimal $C_{1,m}$ at a certain low fraction x_0 of the more volatile component. The experimental values of $C_{1,m}$ are shown to be in quantitative agreement with the theoretical predictions for free or released bubbles. These values have been used previously to study the more complex behaviour during adherence [12]†.

In the mixtures investigated—4·1 wt % methylethylketone ($x_0 = 4{\cdot}1 \times 10^{-2}$) and 1·5 wt % ($x_0 = 1{\cdot}5 \times 10^{-2}$) and 6·0 wt % 1-butanol ($x_0 = 6{\cdot}0 \times 10^{-2}$)—smaller bubbles are generated at higher frequencies in comparison with the less volatile pure component (water). As a

† Same bubbles investigated previously [12] are denoted here by same letters.

consequence, the onset of film boiling occurs then at a very dense bubble population on the heating wire. This is also partly due to the Marangoni-effect, which diminishes the tendency to premature bubble coalescence. The liquid boundary layer is pushed away from the heating wall very frequently, which results in a considerably increased peak flux density, up to a factor three† ("boiling paradox", cf. [12]).

Other reasons for investigating water–methylethylketone and water–1-butanol are [9, 10]: (i) the maximum $q_{w,\,max}$ occurs in a narrow range of completely miscible components; (ii) the corresponding $K = y/x = 17 \gg 1$, and the corresponding maximum $\Delta T/G_d$ can be deduced from equilibrium data, which are known in the literature; and (iii) experimental values of D are also available for water–1-butanol, whence experimental bubble growth rates can be compared with theoretical predictions. For practical purposes, the small, nearly spherical, released bubbles in these mixtures are advantageous in comparison with the larger, more irregular bubbles in water.

The same heat flux density q_w was used in these liquids. This value (45×10^4 W/m^2) was chosen so as to generate a moderate density of active nuclei on the heating surface in the region of nucleate boiling. In this way an eventual change in growth rate of a bubble, due to the presence of near neighbours, could mostly be avoided. A comparison of experimental data on released bubbles with theoretical predictions for free bubbles with the bubble centre at rest is possible now. Actually, this is allowed only for relatively small bubbles, as the ascending velocity of larger bubbles will be increased due to the occurrence of an internal circulation, cf. e.g. [18]. The liquid boundary layer adjacent to a vapour bubble is continuously renewed then, and increased growth rates may be expected. However, this internal circulation has not been observed for small bubbles, whence the original boundary layer will adhere to such ascending bubbles.

The transition from nucleate boiling to film boiling by exceeding gradually the critical temperature difference $\theta_{0,\,max}$ of the azeotropic mixture (95·6 wt % ethanol) of the system water–ethanol, has also been studied [11].

2. APPARATUS AND PROCEDURE

2.1. *Photographic technique*

2.1.1. *High-speed motion picture camera.* A Fairchild HS 101 (30 m, 16 mm film) high speed motion picture camera of the rotating-prism type was operated at 6000 f.p.s. An Elgeet 76 mm, f/1·9 lens was provided with a 50 mm extension tube. A timing light placed marks on the edges of the Ferrania 27 reversal panchromatic cine-film and so an accurate time base is obtained for evaluation of data. A Früngel timing light generator was used, which produces signals of approximately 30 μs duration at a frequency of 1000 c/s. Quantitative measurements were taken from the last 8 m only of an exposed film, as the speed of this portion was constant within 0·5 per cent.

Convenient focussing of the camera is possible by using a boresight viewfinder. The head of a film was elongated by splicing it with a perforated nylon type. A suitable portion of the nylon tape, which faced the objective, was provided with a piece of Scotch mending tape and acted as a focussing screen of good quality. For operation, the camera was screwed tight on a heavy Linhof tripod. The bottom heater of the boiling vessel was placed on a carriage, which could be adjusted with a screw micrometer. This carriage is movable along the optical axis of the camera objective in order to adjust the distance

† These results have been obtained on electrically heated, horizontal platinum wires with a diameter of 2×10^{-4} m, immersed in a relatively large boiling vessel with a heated bottom plate. Lower maxima in mixtures occur generally on wires with much larger diameters and on flat heating plates. This is mainly caused by a local exhaustion of the more volatile component nearby the heating surface or by a lower bubble frequency due to a prolonged adherence to the wall at the same small departure size. The first effect depends on the available liquid volume, and is removed in surface boiling. The latter effect is connected with the flow pattern due to the geometry of the heating surface.

from the heating wire to the focussing screen on the film.

2.1.2. *Illumination.* A 24 V/500 W radium over-run lamp was operated at 30 V a.c., so as to achieve increased illumination. The filament of the incandescent lamp was located at the focus of a Hessenbruch parabolic mirror. The metal-coated front of the inside of the glass bulb acted also as a mirror, reflecting the light, which travelled originally in the forward direction. In this way a beam of parallel rays was obtained, which was focused by a separate Rodenstock converging lens on a vertical ground glass. This intensively illuminated screen was placed in the boiling vessel, a few millimeters behind the heating wire and a calibrated 2-mm scale (Fig. 1). Thus the contours of vapour bubbles

Another feature of against-the-light photography is that nearly all the light is scattered in the general forward direction, in the case of a beam of parallel rays incident upon a spherical vapour bubble. This method of observation has advantages here, compared to front lighting, as an aperture setting f/5·6 could be used, resulting in a larger depth of field and a higher resolving power of the large-aperture objective.

2.2. *Boiling vessel*

Optically parallel glass windows and polytetrafluoroethylene (at the inside of the vessel) and neoprene rubber (for the outside of the glass windows) packing has been used. A total reflux condenser was mounted on the removable cover plate. The vessel was partly filled with

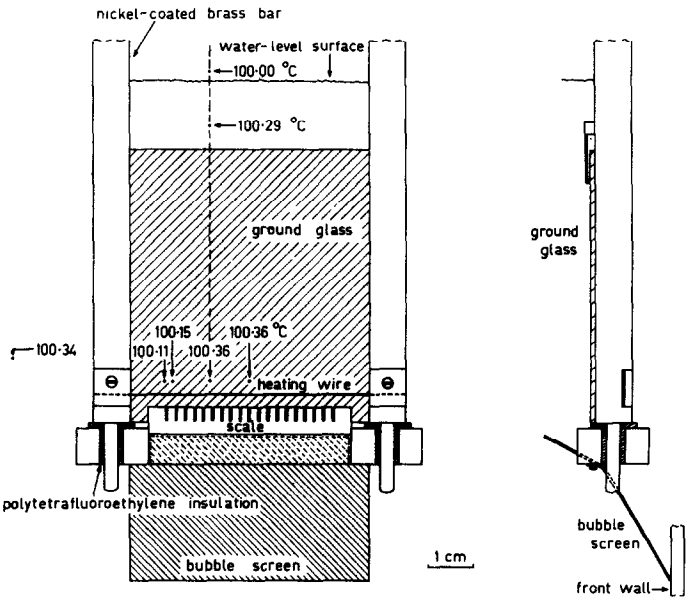

FIG. 1. Sections of parts of boiling vessel showing temperature distribution in *water* boiling at atmospheric pressure.
The nucleate boiling heat flux density of the platinum wire was 45×10^4 W/m^2 and the power of the bottom heater was 100 W.

distinct on the photographs giving maximum contrast between the interior of the bubbles and their surroundings on account of total reflection.

liquid and heated at the base by an electric heater. Uniform boiling was maintained, as heat losses were compensated by this heater. Liquid

temperatures were measured with a calibrated mercury-in-glass thermometer, small temperature differences (e.g. liquid superheatings) with a calibrated copper–constantan thermocouple, consisting of thin wires. An a.c. was passed through the horizontal, "physically pure" (99·99 per cent) platinum heating wire, which acted as the heating surface. The heat flux density was calculated from the electric power:

$$q_w = \frac{EI}{\pi L_w D_w}. \tag{1}$$

A constant $q_w = 45 \times 10^4$ W/m^2 was chosen, which corresponded to a power of 15 W. The power of the bottom heater was adjusted to 100 W for taking motion pictures.

Boiling curves (including wire superheatings θ_0) were obtained previously by passing a stepwise increasing d.c. through the wire (with a diameter of 2×10^{-4} m), of which a central portion was isolated as a test section by making use of thin platinum potential taps with diameters of 5×10^{-5} m. This section served as the heating surface and at the same time as a resistance thermometer [19].

2.3. *Evaluation of bubble dimensions*

The field of view of the camera was determined by selecting a suitable combination of lens and extension tube (Section 2.1.1). The boiling vessel was provided with a calibrated 2-mm scale for evaluation of bubble dimensions. The vapour bubbles investigated were viewed by a tenfold (water) to fiftyfold (mixtures) linear enlargement in comparison to real dimensions.

An ascending free vapour bubble was approximated by a rotation ellipsoid, in agreement with the theory by Siemes [20] for bubbles with radii up to 3×10^{-3} m. The rotation axis coincides with the direction of the flow of the surrounding liquid (in most cases vertical).

Several bubbles oscillated about the spherical shape. The most frequently observed mode of vibration is the slowest, fundamental harmonic. In this case a sphere is transformed periodically into a rotation ellipsoid with $a_1 > a_2$ and $a_1 < a_2$, respectively.

It is obvious now that one has to determine the equivalent bubble radius R (of a sphere with the same volume) from:

$$R = (a_1^2 a_2)^{\frac{1}{3}} \approx \frac{2a_1 + a_2}{3}. \tag{2}$$

The values following from the approximation in the right-hand side of equation (2) are not more than 0·5 per cent (second-order deviation) too large in comparison with the left-hand side for bubbles with $0{\cdot}8 \leqslant a_1/a_2 \leqslant 1{\cdot}2$, cf. Fig. 30.

3. THE SUPERHEATING OF THE BULK LIQUID

3.1. *Water*

In order to keep out of vision vapour bubbles, moving upwards from the front side of the heated bottom plate of the boiling vessel, a metal sheet was attached to the ends of the scale. This screen inclined downwards in the direction to the front wall of the vessel (Fig. 1). The front bubbles rise now behind the ground glass to the liquid-level surface and are no longer inconvenient obstacles in the field of vision.

The superheating was measured along a line parallel to the heating wire 3 mm above it. This superheating was no longer constant, but varied from 0·11–0·36 degC for a nucleate boiling heat flux density of $q_w = 45 \times 10^4$ W/m^2 as a consequence of the presence of the ground glass and the bubble screen ($\Delta\theta_0 = 0{\cdot}36$ degC is the value in absence of ground glass and screen, i.e. representative for commonly used boiling vessels). The superheating of the bulk liquid, which was determined with a mercury-in-glass thermometer, amounted to 0·34 degC. The bottom heater was adjusted to a power of 100 W, a part of which is lost to the surroundings. The ends of the platinum wire were to some extent outside the main flow of the boiling water, ascending from the heated bottom of the vessel (cf. Fig. 1). This results in different growth rates of vapour bubbles after breaking away from the platinum wire.

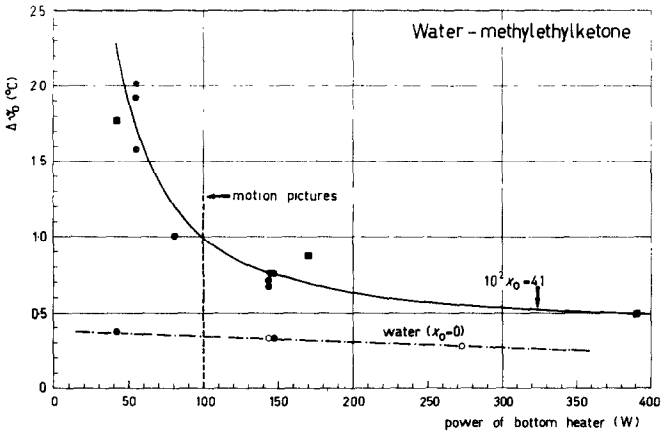

FIG. 2. Superheating of *water* and of 4·1 wt % *methylethylketone* boiling at atmospheric pressure. Superheatings are measured at a distance of approximately 3 mm above the centre of the platinum wire.
Water: ● boiling vessel provided with ground glass and bubble screen; ○ ground glass and bubble screen removed.
4·1 wt % *methylethylketone*: boiling vessel provided with ground glass and bubble screen.
Experiments carried out in the same run are represented by the same figures.

For the boiling vessel with removed ground glass and bubble screen, a heat flux density of only 300 W/m^2, transmitted by the bottom heater, should have been sufficient to maintain a constant superheating in the entire bulk liquid, according to Jakob and Fritz [1], cf. Section 1.2 and Fig. 1 of Part I [2].

Jakob and Fritz have also shown that the superheating of the bulk liquid is independent of the heat flux of the bottom heater, at least in the lower part of the region of nucleate boiling for water at atmospheric pressure. Their results are in agreement with Fig. 2: the superheating decreases only slightly by increasing the heat flux density of the bottom heater. This will be connected with the rate, at which the number of vapour bubbles, generated per second and per unit area on active nuclei at the heating surface, increases.

3.2. *Water–methylethylketone*

In 4·1 wt % methylethylketone [9, 10] the effect of measuring higher superheatings along the centre of the horizontal line 3 mm above the heating wire has apparently been removed (Fig. 3). The same value of the bubble growth

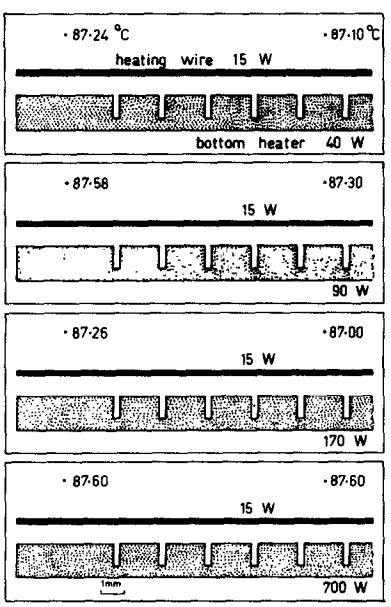

FIG. 3. 4·1 wt % *methylethylketone*. Temperature distribution above heating wire in binary mixture boiling at atmospheric pressure, for different powers of bottom heater.

factor $C_{2,m}$ occurs for released bubbles, independent of the location of the generating nucleus at the wire surface (cf. Fig. 13).

Also, in contrast to the behaviour in water, the superheating of bulk liquid in this mixture decreases considerably, especially in the range of low heat fluxes (Fig. 2). This effect may be due to a more rapid increase in the number of active nuclei, in comparison to water.

3.3. *Water–1-butanol*

The superheating in a mixture depends on the power of the bottom heater (Fig. 4). The curve

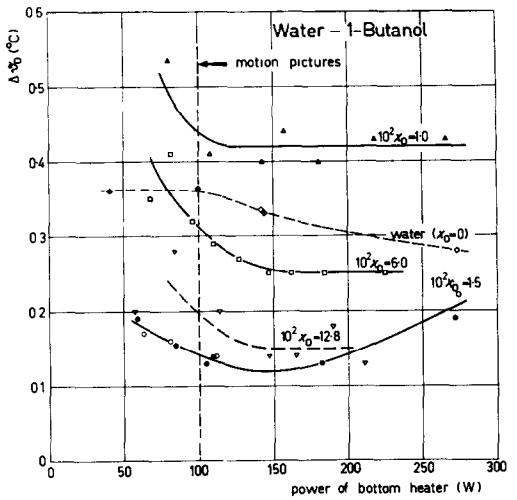

FIG. 4. *Water–1-butanol.* Superheating of mixtures; % denotes wt % 1-butanol. Superheatings were measured approximately 3 mm above the centre of the (same) platinum heating wire, or above the right nucleus (in 6·0%). Reproducibility of results is shown for 1·5%; cold junction of copper–constantan thermocouple in he vapour space at a distance of 2·5 mm above the liquid-level surface ● or at 5 mm ○, cf. Figs. 1 and 2 of Part I.
The boiling vessel was provided with ground glass and bubble screen, with the exception ◇ for water.

for 1·5 % wt 1-butanol shows a minimum at a power of 150 W [10]. The liquid superheating is shown in Fig. 5 in dependence on composition. The power of the external heater was taken constant here at 100 W (motion pictures) or 150 W (minimum superheatings).

During the tests reported here, the motion pictures show released vapour bubbles in liquids with superheatings: varying from 0·11–0·36 degC for water; constant at a value of 0·95 degC for 4·1 wt % methylethylketone and constant at 0·14 degC for 1·5 wt % 1-butanol, and 0·31 degC for 6·0 wt % 1-butanol.

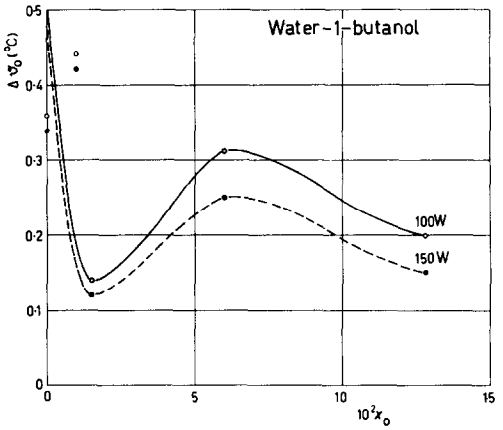

FIG. 5. *Water–1-butanol.* Superheating as a function of composition at constant heater power and constant nucleate boiling heat flux density of wire (45×10^4 W/m^2).
A minimum superheating occurs at 1·5 wt % and a maximum at 6·0 wt % of 1-butanol in both curves.

Experimental data can easily be compared with $C_2 = C_1^{**}(\Delta\theta_0)^{0.75}$, cf. Fig. 6 of Part I [2], but preference is given here to the exact equation (15), i.e. equation (71) of Part I [2], cf. Section 6.4.

4. EXPERIMENTAL BUBBLE GROWTH IN WATER IN COMPARISON WITH THEORETICAL PREDICTIONS

The size of bubbles breaking away from various nuclei on the wire differs considerably (cf. Figs. 6–8). Intentionally, "growth curves" $R(t)$ have been determined for some relatively large and for some smaller bubbles. The radii of three successive bubbles, generated on the same nucleus, are shown as a function of time in Fig. 7. The bubbles oscillate both in shape and in volume, cf. the Appendix on bubble vibrations.

The slope of the curves for adhering bubbles in Fig. 7 decreases continuously, in good agreement with van Stralen's relaxation microlayer theory [12]. The curves for released bubbles are compared with the theoretical growth of free

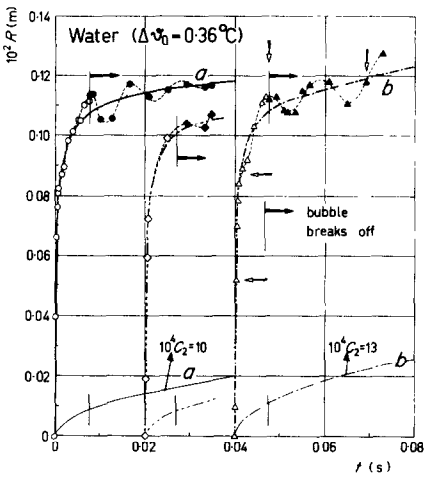

FIG. 7. *Water.* Growth of consecutive vibrating bubbles, generated on the same nucleus; $\Theta_0 = 20$ degC and $\Delta\theta_0 = 0{\cdot}36$ degC.

The curves $R = 10 \times 10^{-4} t^{\frac{1}{2}}$ (bubble *a*) and $R = 13 \times 10^{-4} t^{\frac{1}{2}}$ (bubble *b*), at the bottom of the figure, denote theoretical growth of free bubbles, which are subjected only to the superheating of bulk liquid. The arrows at the curve for bubble *b* denote the frames shown in Fig. 9.

bubbles, which are subjected to a constant superheating $\Delta\theta_0$ of bulk liquid only. The dotted curves are parabolas, cf. Part I [2]:

$$R_p(t) = C_{2,p}\, t^{\frac{1}{2}} \cong C_1\, \Delta\theta_0\, t^{\frac{1}{2}}, \qquad (3)$$

where the theoretical value for asymptotic growth of $C_{1,p} = 24 \times 10^{-4}$ m/s$^{\frac{1}{2}}$ degC according to Plesset and Zwick and $C_{1,p} = 22 \times 10^{-4}$ m/s$^{\frac{1}{2}}$ degC according to Forster and Zuber, cf. Part I [2].

The contrast with the rapid initial growth of bubbles adhering to the wire with a superheating $\theta_0 = 20$ degC is striking. One has during adherence [12]:

$$R_p(t) = bC_{1,p}\,\theta_0\, t^{\frac{1}{2}} \exp -\left(\frac{t}{t_1}\right)^{\frac{1}{2}} \qquad (4)$$

and hence for the departure radius:

$$R_{1,p} = R_p(t_1) = \frac{b}{e} C_{1,p}\,\theta_0\, t_1^{\frac{1}{2}}. \qquad (5)$$

For comparison with the theoretical equation (3), growth curves were plotted, showing the radius R of released bubbles as a function of $t^{\frac{1}{2}} - t_1^{\frac{1}{2}}$ (Fig. 8); t_1 may differ for bubbles of

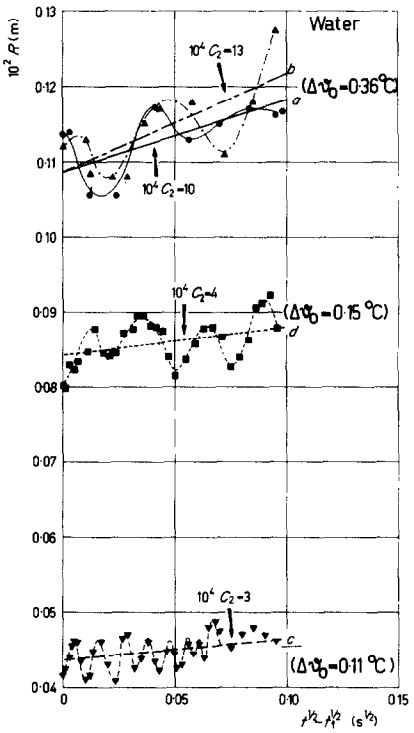

FIG. 8. *Water.* Growth curves for vibrating vapour bubbles, after departure. $\Delta\theta_0 = 0{\cdot}36$ degC for bubbles *a* and *b*, $\Delta\theta_0 = 0{\cdot}15$ degC for bubble *d*, and $\Delta\theta_0 = 0{\cdot}11$ degC for bubble *c*.

various dimensions. However, a translation of a growth curve has no effect on the slope.

The frequency of bubble formation amounted exactly to 50 s^{-1}. This may be a consequence of the use of a.c. A similar effect was observed by Faneuff, McLean and Scherrer [21] heating nichrome wires with electrical short duration repetitive pulses. The bubbles adhere to the surface during a time $t_{1,p} = 8 \times 10^{-3}$ s before

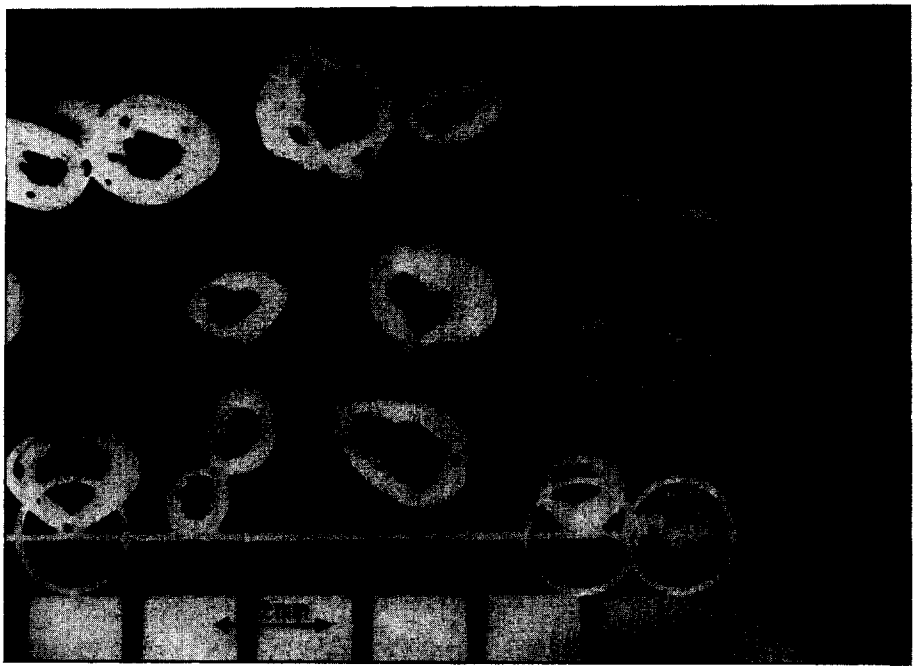

FIG. 6. *Water*. Field of view of high-speed motion picture camera, provided with 76 mm lens and 50 mm extension tube. A calibrated 2-mm scale was used for evaluation of bubble dimensions. The consecutive bubbles *a* and *b* were formed on the left nucleus ($\Delta\theta_0 = 0{\cdot}36$ degC), bubble *d* on the intermediate nucleus ($\Delta\theta_0 = 0{\cdot}15$ degC) and bubble *c* on the right nucleus ($\Delta\theta_0 = 0{\cdot}11$ degC).

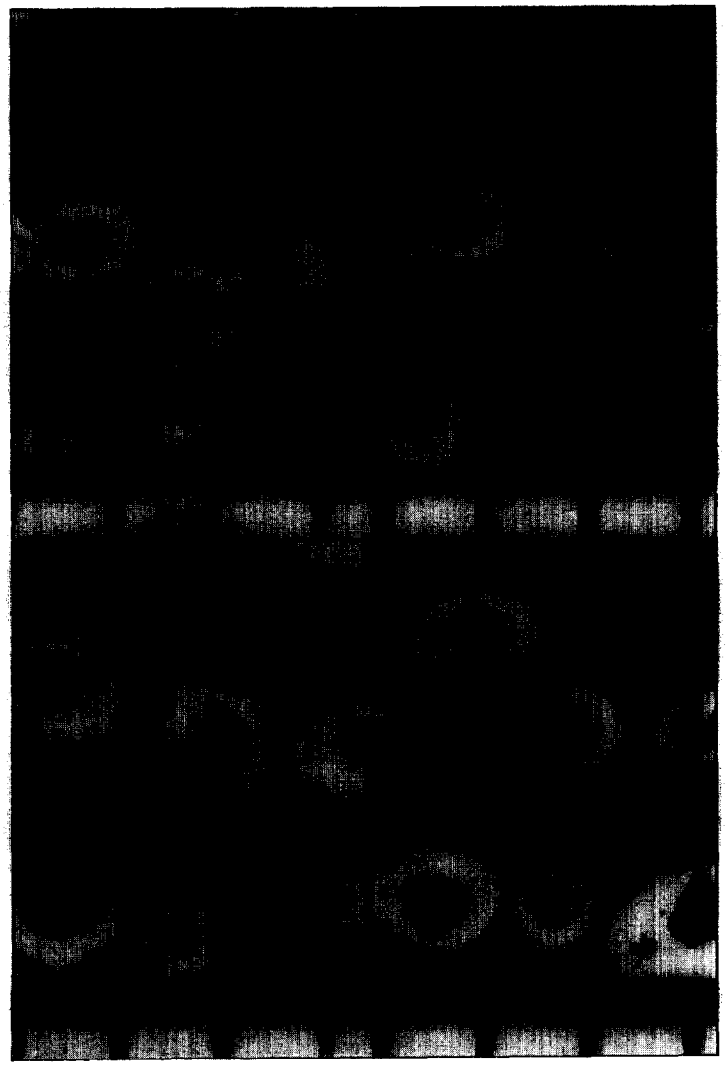

FIG. 9. *Water*. Photographs showing the growth of the vibrating bubble *b* of Figs. 7 and 8.
1 = frame no. 2; 2 = frame no. 9; 3 = frame no. 44; 4 = frame no. 175. Time interval between successive pictures is $1{\cdot}67 \times 10^{-4}$ s. Camera speed 6000 f.p.s. Frame no. 0 shows no bubble on the nucleus. Frame no. 44 shows the bubble at the instant of breaking away from the heating surface. A 2-mm scale is visible at the bottom of the photographs.

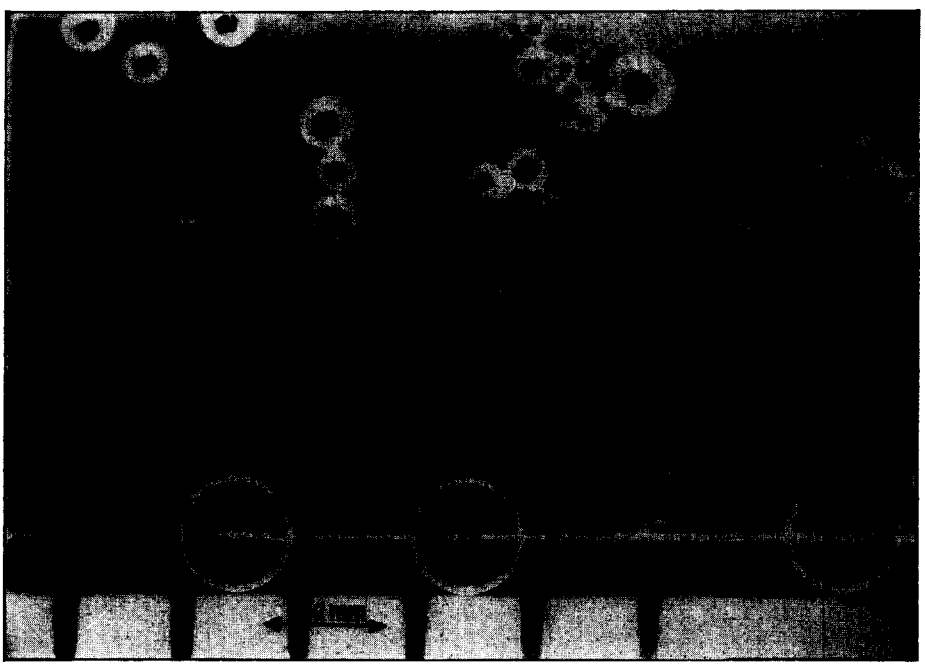

FIG. 10. 4.1 wt % *methylethylketone*. Field of view of camera. The consecutive bubbles *a* and *b* originate from the left nucleus and bubble *c* from the right nucleus. Bubbles *d* and e are formed in the liquid above the intermediate nucleus.

A striking feature is the reduced size of vapour bubbles in this mixture in comparison to water, cf. Fig. 6. Sometimes tiny bubbles are breaking away downwards from the intermediate nucleus. A 2-mm scale is visible at the bottom.

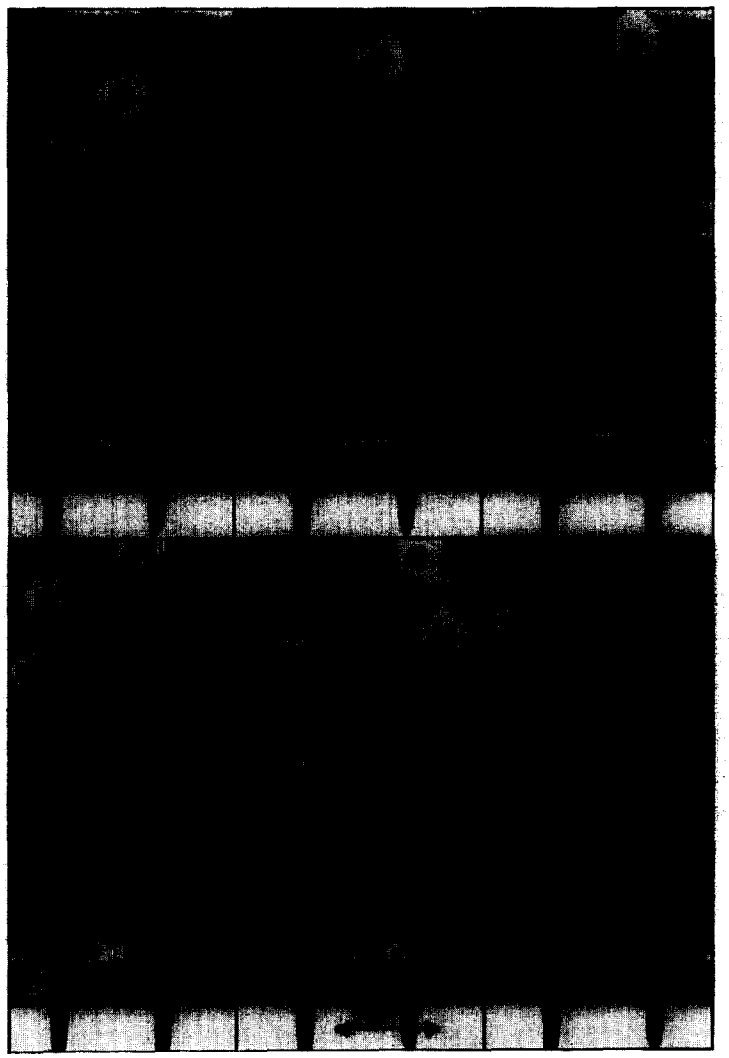

FIG. 12. 4.1 wt % *methylethylketone*. Photographs showing the growth of the vibrating bubble *a* of Figs. 11, 13 and 30.

1 = frame no. 1; 2 = frame no. 23; 3 = frame no. 34; 4 = frame no. 43; 5 = frame no. 172; 6 = frame no. 267. Time interval between successive pictures is $1{\cdot}67 \times 10^{-4}$ s. Frame no. 0 shows no bubble on the nucleus. Frame no. 43 shows the bubble shortly before breaking away from the heating surface. A 2-mm scale is visible at the bottom of the photographs.

The succeeding bubble *b* is shown also in photographs 5 and 6.

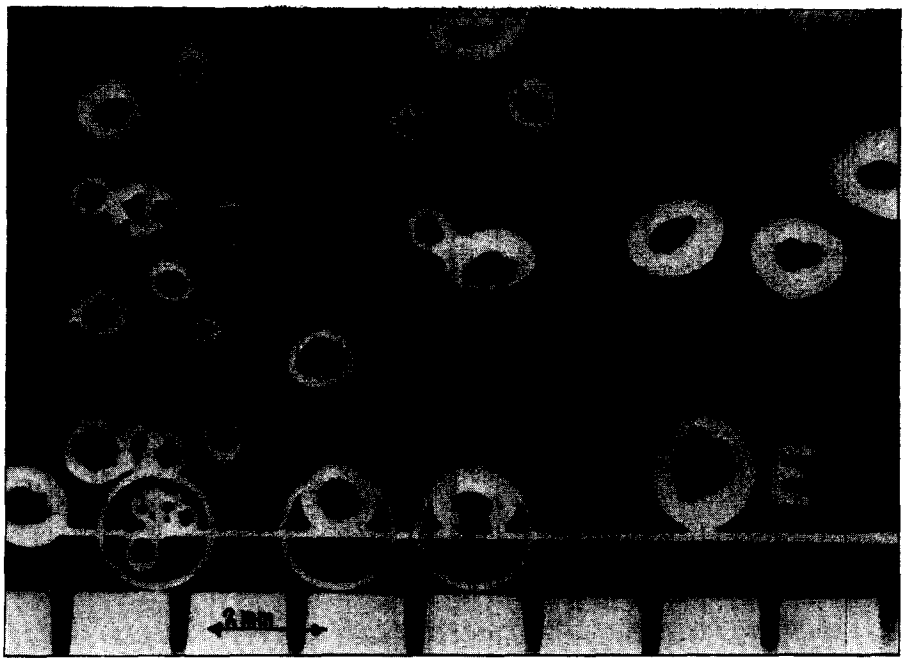

FIG. 15. 1·5 wt % 1-*butanol*. Field of view of high-speed motion picture camera, provided with 76-mm lens and 50-mm extension tube. A 2-mm scale was used for evaluation of bubble dimensions.

Bubble e is shown one frame before the instant of breaking away from the heating surface (i.e. frame no. 68 of bubble e). The consecutive bubbles *b*, *c* and *d* and bubble *a* are formed on the nucleus at the centre of the wire ($\Delta\theta_0 = 0{\cdot}14$ degC), bubble *h* on the left nucleus and bubble *f* on the intermediate nucleus. The nucleus generating bubble *g* is located at 0·1 cm to the left of the nucleus generating bubble *a*. That nucleus was not active at the instant of taking this frame.

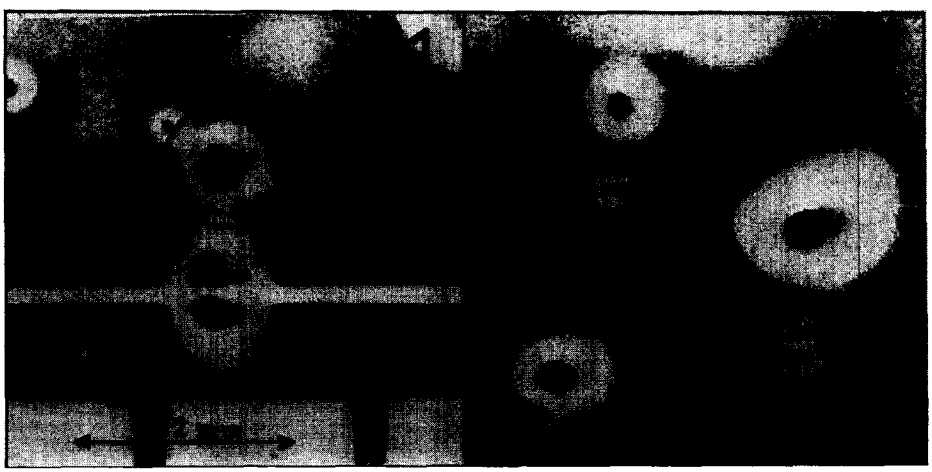

FIG. 18. 1·5 wt % 1-*butanol*. Photographs showing the growth of bubble *f* in Fig. 17.

1 = frame no. 72; 2 = frame no. 204 = frame no. 22 of bubble *c*, of Fig 16. Time interval between successive pictures is $1{\cdot}67 \times 10^{-4}$ s. Frame no. 0 shows no bubble on the nucleus. A 2-mm scale is visible at the bottom of photograph 1.

1: the growth of bubble *f* (in black circle) is stopped completely due to its close proximity to another bubble, which grows rapidly at the heating surface; 2: bubble *f* is growing again.

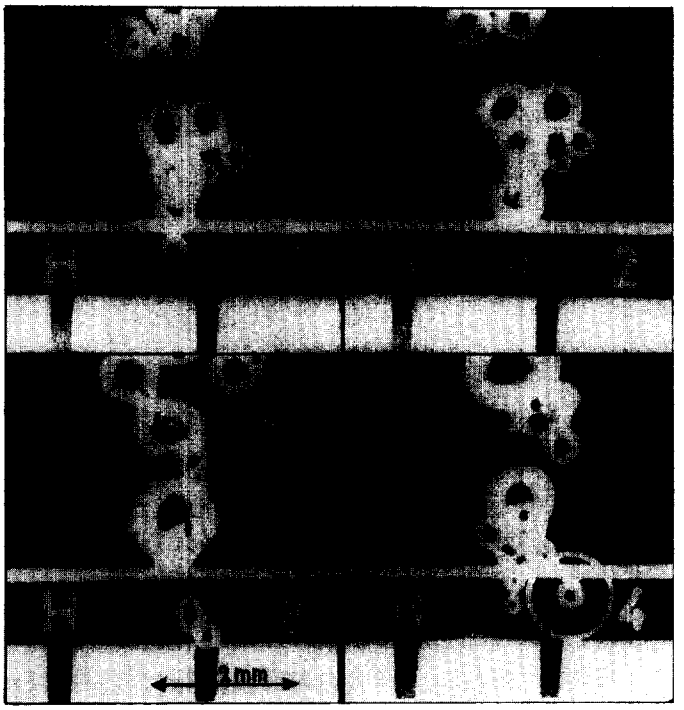

FIG. 19. 1·5 wt % 1-*butanol*. Photographs showing the growth of bubble *h* in Fig. 17.

1 = frame no. 11; 2 = frame no. 21; 3 = frame no. 62; 4 = frame no. 125. Time interval between successive pictures is $1{\cdot}67 \times 10^{-4}$ s. Frame no. 0 shows no bubble on the nucleus. A 2-mm scale is visible at the bottom of the photographs.

1: bubble *h* at the instant of breaking away downwards from the heating wire; 3: bubble *h* between the scale; 4: the bubble moves upwards and meets the wire again.

The growth factor $C_{2,m} = 0$ for this bubble after release due to the competitive consumption of the more volatile component by neighbouring bubbles, generated on the wire.

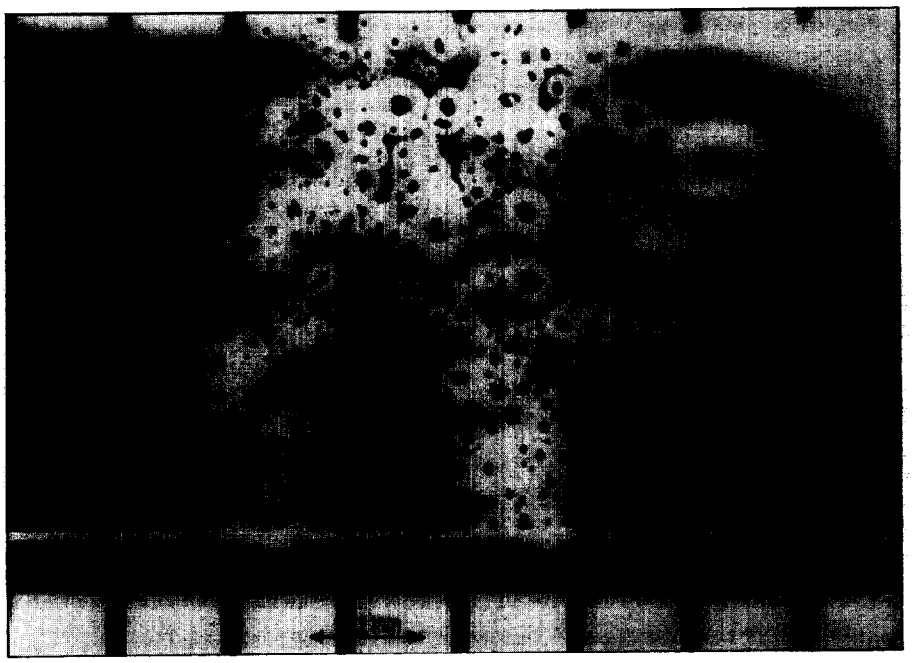

FIG. 20. 6·0 wt % 1-*butanol*. Field of view of camera. A 2-mm scale is visible at the bottom of the photograph, which shows frame no. 1 of bubble *a* = frame no. 198 of bubble *c*.

The bubbles investigated are generated on the right nucleus. The initial growth rates of bubbles on the other nuclei could not be determined owing to the dense bubble population.

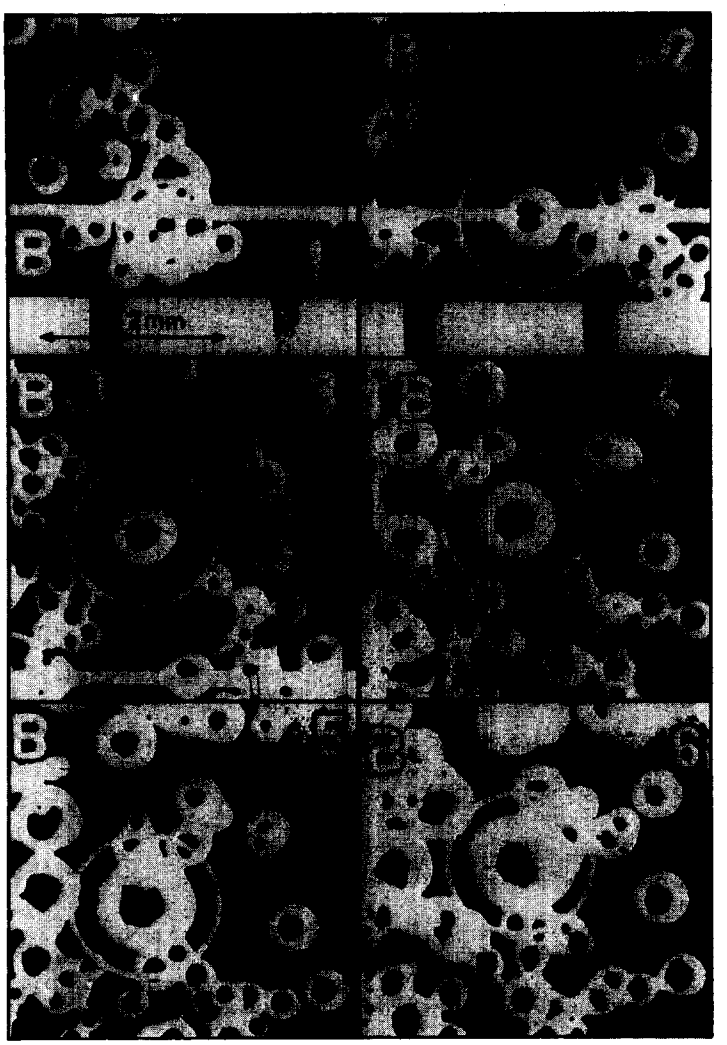

FIG. 23. 6·0 wt % 1-*butanol*. Photographs showing the growth of bubble *b* in Fig. 21.

1 = frame no. 1; 2 = frame no. 189; 3 = frame no. 240; 4 = frame no. 278; 5 = frame no. 326; 6 = frame no. 383. Time interval between successive pictures is $1{\cdot}67 \times 10^{-4}$ s. Frame no. 0 shows no bubble on the nucleus. A 2-mm scale is visible at the bottom of photographs 1 and 2.

1, 2: bubble *b* grows after release according to $R = 6{\cdot}5 \times 10^{-4} t^{\frac{1}{2}}$ with $\Delta\theta_0 = 0{\cdot}31$ degC; 3, 4: bubble *b* grows rapidly owing to a movement outside the domain of competitive consumption of the more volatile component by neighbouring bubbles; 5, 6: the growth has again been slowed down.

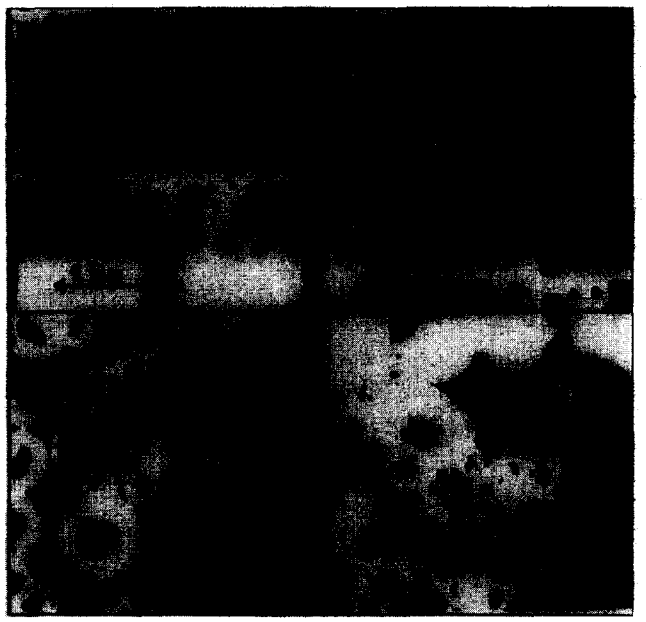

FIG. 24. 6·0 wt % 1-*butanol*. Photographs showing the growth of bubble e in Fig. 21.

1 = frame no. 32; 2 = frame no. 157; 3 = frame no. 240; 4 = frame no. 319. Time interval between successive pictures is $1{\cdot}67 \times 10^{-4}$ s. Frame no. 0 shows no bubble on the nucleus. A 2-mm scale is visible at the bottom of photograph 1.

1, 2: bubble e grows according to $R = 6{\cdot}5 \times 10^{-4}\, t^{\frac{1}{2}}$ with $\Delta\theta_0 = 0{\cdot}31$ degC; 3: growth of bubble e is stopped owing to its close proximity to two larger bubbles; 4: bubble e is growing again.

breaking off. An uncertainty of up to maximally $1{\cdot}7 \times 10^{-4}$ s occurs in the determination of the instant at which a bubble starts to grow from the equilibrium radius R_0, as this time lies between the first visible bubble picture and the exactly preceding frame showing no bubble.

From Figs. 7 and 8 the following experimental values of the growth coefficient, $C_{2,p}$, are found:

Initial growth: $C_{2,p}(\theta_0) \approx 500 \times 10^{-4}$ m/s$^{\frac{1}{2}}$, with $\theta_0 = 20$ degC. (6)

Growth after release: $C_{2,p}(\Delta\theta_0) = 11{\cdot}5 \times 10^{-4}$ m/s$^{\frac{1}{2}}$, with $\Delta\theta_0 = 0{\cdot}36$ degC, i.e. $C_{1,p} = 32 \times 10^{-4}$ m/s$^{\frac{1}{2}}$ degC; $C_{2,p} = 4 \times 10^{-4}$ m/s$^{\frac{1}{2}}$, with $\Delta\theta_0 = 0{\cdot}15$ degC, and $C_{2,p} = 3 \times 10^{-4}$ m/s$^{\frac{1}{2}}$, with $\Delta\theta_0 = 0{\cdot}11$ degC. (7)

which are described in the literature, may occur as a consequence of coalescence.

The average value of $R_{1,p} = 9{\cdot}2 \times 10^{-4}$ m at $\theta_0 = 20$ degC. Hence the growth parameter $b = 0{\cdot}70$ in equation (5), cf. [12].

5. BUBBLE GROWTH IN 4·1 WT % METHYLETHYLKETONE

5.1. *Experimental results*

The photographs in Figs. 10 and 12 for 4·1 wt % methylethylketone illustrate the slowing down of bubble growth and decreased bubble size at the instant of breaking away from the heating wire, in contrast to Figs. 6 and 9 for water. For this mixture similar $R(t)$-curves have been obtained as for water (Figs. 11 and 13). Bubbles *a* and *b*, which were formed on the same

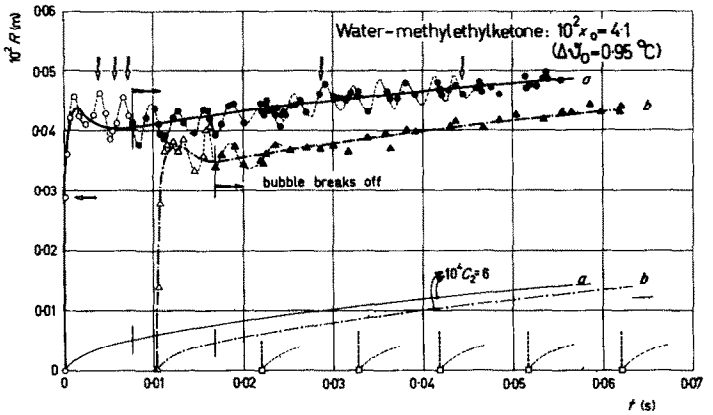

FIG. 11. 4·1 wt % *methylethylketone.* Growth of successive vibrating vapour bubbles, generated on the same nucleus; $\vartheta_0 = 24$ degC and $\Delta\theta_0 = 0{\cdot}95$ degC. The curves $R = 6 \times 10^{-4}\, t^{\frac{1}{2}}$ at the bottom of the figure denote growth of free bubbles, which are subjected only to the superheating of bulk liquid. Arrows on curve for bubble *a* denote the frames shown in Fig. 12.

These experimental results are in good agreement with Scriven's theoretical predictions, cf. Fig. 5 of Part I [2].

In Fig. 9 some characteristic motion pictures show the growth of bubble *b* of Figs. 7 and 8. In photograph 2 some touching bubbles coalesce, in photograph 4 the successor of bubble *b* on the same nucleus has already been released from the wire. Complicated bubble shapes, nucleus, vibrate similarly to bubbles in water (Figs. 11 and 13).† The time between the formation of two consecutive bubbles on the nucleus generating bubbles *a* and *b*, amounts to $1{\cdot}04 \times 10^{-2}$ s. The time of adherence to the wire $t_1 = 7 \times 10^{-3}$ s, i.e. approximately only 10 per

† The reader is referred to the Appendix on bubble vibrations; especially the behaviour of bubble a in 4·1 wt % methylethylketone is studied (Fig. 30).

cent shorter than for the larger bubbles *a* and *b* in water (cf. Fig. 7 and Parts I and II of [12]).

The initial growth rate of bubbles in 4·1 wt % methylethylketone corresponds to a wire superheating $\theta_0 = 24$ degC, the growth rate for released bubbles to a superheating of bulk liquid $\Delta\theta_0 = 0{\cdot}95$ degC (Fig. 2).

Bubbles generated on a nucleus, which is located at the lower side of the heating wire, creep slowly upward, while they remain attached to the surface. This is also the case in water. Sometimes, however, tiny bubbles leave the wire in the direction perpendicular to the surface. Hence some small bubbles move downward immediately after breaking away from the surface (cf. Fig. 10). The average size of releasing bubbles is smaller than in water, cf. equation (5) These effects cannot be explained by using current equations in the literature [1], which are based on the decrease in surface tension in comparison to water. A quantitative explanation in terms of equation (5) follows from van Stralen's relaxation microlayer theory [12].

The growth rate of bubbles *a* and *b* is high during an initial stage of 2×10^{-3}s. During the next 5×10^{-3}s before departure, their growth is stopped completely, or, more exactly, even a condensation of short duration occurs, cf. Section 5.2.2. For released (vibrating) bubbles *a* and *b*, Figs. 11 and 13, and (nonvibrating) bubble *c*, Fig. 13, one finds:

$$C_{2,m} = C_{1,m}\Delta\theta_0 = 6 \times 10^{-4}\text{m/s}^{\frac{1}{2}}, \quad \text{with } \Delta\theta_0 = 0{\cdot}95 \text{ degC}. \tag{8}$$

Hence

$$C_{1,m} = 6 \times 10^{-4}\text{m/s}^{\frac{1}{2}}\text{ degC}. \tag{9}$$

The ratio of these values of $C_{2,m}$ and $C_{1,m}$ to the corresponding values in water, cf. equations (6) and (7) shows a decrease to approximately 50 per cent and 20 per cent, respectively. More exactly, one has in the bubble growth equation $R = C_2 t^{\frac{1}{2}}$:

$$C_2 \sim (\Delta\theta_0)^n. \tag{10}$$

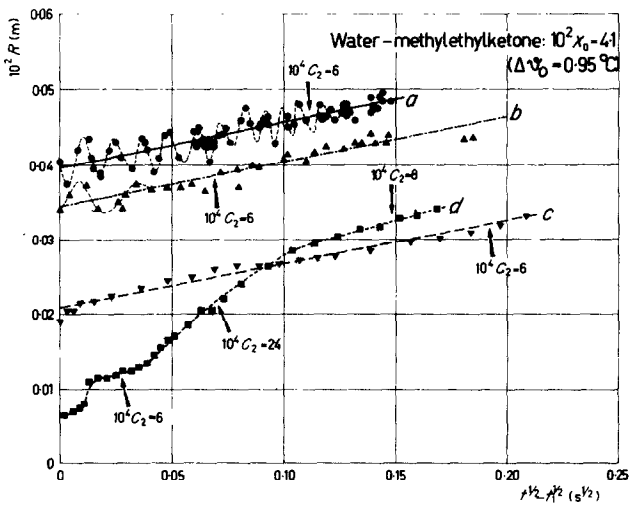

FIG. 13. 4·1 wt % *methylethylketone*. Growth curves for vapour bubbles after departure. Bubbles *a* and *b* (vibrating) and bubble *c* (nonvibrating) are generated on the heating wire, bubble *d* (nonvibrating) was formed in the liquid above the wire, cf. Fig. 10; $\Delta\theta_0 = 0{\cdot}95$ degC.

The growth of bubble *d* is sometimes increased due to its movement in the forward direction, outside the range of neighbouring bubbles.

A value of the exponent is found: $n = 0{\cdot}80$ at $\Delta\theta_0 = 0{\cdot}36$ degC (water) and $n = 0{\cdot}90$ at $\Delta\theta_0 = 0{\cdot}95$ degC (4·1 wt % methylethylketone), cf. Fig. 6 of Part I[2]. The constant of proportionality in equation (10) amounts to 27×10^{-4}m/s$^{\frac{1}{2}}$ degC$^{0{\cdot}85}$ in water and to 6×10^{-4}m/s$^{\frac{1}{2}}$ degC$^{0{\cdot}85}$ in the mixture by taking the average $n = 0{\cdot}85$, i.e. the experimental value of this growth constant is reduced to 22 per cent.

The growth curve for bubble *d* in Fig. 13 shows two parts with an increased slope. This is because this bubble moved forward, outside the range of competitive consumption of the more volatile component by neighbouring bubbles. In the main region of this curve the growth factor $C_2 = 24 \times 10^{-4}$m/s$^{\frac{1}{2}}$, i.e. nearly equal to the value in water at $\Delta\theta_0 = 0{\cdot}95$ degC, cf. Fig. 5 of Part I [2].

Two growth curves have been plotted for bubble *e* in Fig. 14. This bubble was initially

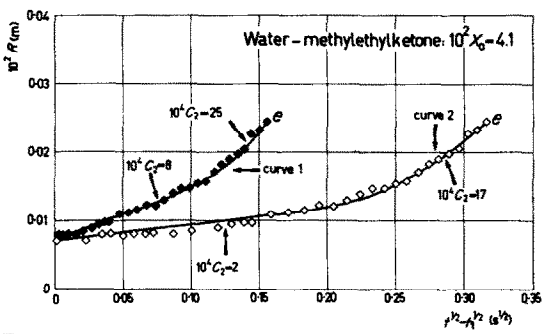

FIG. 14. 4·1 wt % *methylethylketone.* Extreme growth curves for a (nonvibrating) bubble *e*, which is formed in the boiling liquid above the heating wire, cf. Fig. 10.

Curve 1: time t was taken from linear extrapolation to zero bubble dimensions at the constant superheating of bulk liquid; t_1 is here the time of the first clearly visible bubble picture.

Curve 2: time t was measured from the first visible bubble picture; $t_1 = 0$ in this case.

formed in the slightly superheated liquid, and not at an active nucleus on the heating wire. The instant of first formation of this bubble is uncertain.

Hence two extreme cases have been considered: For curve 1 this instant has been estimated by means of linear extrapolation to zero dimensions at the constant superheating of bulk liquid. For curve 2 a higher, yet unknown, initial growth rate was assumed; the most extreme case was considered here by taking zero time at the first clearly visible bubble picture.

In this way two limits have been determined for the growth factor, viz. 2×10^{-4}m/s$^{\frac{1}{2}} \quad C_2 \leqslant 8 \times 10^{-4}m/s^{\frac{1}{2}}$ for the lower part of the curves, and 17×10^{-4}m/s$^{\frac{1}{2}} \leqslant C_2 \leqslant 25 \times 10^{-4}$ m/s$^{\frac{1}{2}}$ for the upper part of the curves, where the bubble grows more rapidly for the same reason as bubble *d*, cf. Fig. 13. The average value in the lower part of the curves (5×10^{-4}m/s$^{\frac{1}{2}}$) for this free, nonvibrating bubble deviates only slightly from the value in equation (8) for released bubbles, of which the instants of initial formation and breaking off could be determined nearly exactly.

5.2. *Comparison with theory*

5.2.1. *The bubble growth constant.* A theoretical growth equation for bubbles in mixtures, which is valid for moderate liquid superheatings, has been derived in Part I [2], equation (74):

$$R_m = C_{2,m}\, t^{\frac{1}{2}} \cong C_{1,m}\, \Delta\theta_0\, t^{\frac{1}{2}} = \left(\frac{12}{\pi}\right)^{\frac{1}{2}} \frac{a^{\frac{1}{2}}}{(\rho_2/\rho_1)\{l/c + (a/D)^{\frac{1}{2}}\, \Delta T/G_d\}}\, \Delta\theta_0\, t^{\frac{1}{2}}. \tag{11}$$

A maximum $\Delta T/G_d = 180$ degC is deduced graphically for 4·1 wt % methylethylketone from equilibrium data, cf. Section 2.4 of Part II of [12].

Data of the diffusion constant for methylethylketone in water are not known in the literature. If the value of the diffusion constant for 1-butanol in water ($D = 9{\cdot}7 \times 10^{-10}$m^2/s) at the atmospheric boiling point ($T = 362$°K of 4·1 wt % methylethylketone) is accepted for methylethylketone, on ground of similarity of the molecules, one calculates

$$\mu = \left(\frac{a}{D}\right)^{\frac{1}{2}} = 13{\cdot}2. \tag{12}$$

Hence, the bubble growth constant $C_{1,m}$ in equation (11) for 4·1 wt % methylethylketone

would be reduced to 0·20 of the value in water. This in quantitative agreement with the experimental results. The average departure radius at $\theta_0 = 24$ degC is decreased to $R_{1,m} = 3{\cdot}4 \times 10^{-4}$m, when $R_{1,m} = 0{\cdot}35\ R_{1,p}$ and the growth parameter $b = 0{\cdot}90$ in equation (5), cf. [12].

It may be worth reporting here, that in principle a new method for measurement of the diffusion constant at various temperatures and concentrations can be based on investigations of bubble growth rates in binary mixtures.

5.2.2. *Bubble condensation.* A condensation like that of the adhering bubbles *a* and *b* (Section 5.1) is observed, but only in mixtures. Apparently, this effect must thus be explained only in terms of mass diffusion of the more volatile component. Condensation of the bubble can occur only, if the instantaneous vapour temperature exceeds the instantaneous liquid temperature of the adjacent relaxation microlayer [12]; i.e. only if {cf. equation (69) and Section 2.3.1. of Part I [2]};

$$T(y) = T(x_0) + \left(1 - \frac{C_{1,m}}{C_{1,p}}\right)\theta_0 > T(x_0) + \theta_0 \exp - (t/t_{1,m})^{\frac{1}{2}}. \quad (13)$$

This condition is satisfied in case of $C_{1,m} = 0{\cdot}20\ C_{1,p}$ (Section 5.1) as $(t/t_{1,m})^{\frac{1}{2}} > 0{\cdot}22$. Actually, however, the situation is more complex, as the liberated heat of condensation results in an instantaneous increase of the temperature of the relaxation microlayer.

For pure liquids, equation (13), which is based on the assumption of thermodynamic equilibrium at the bubble interface, is simplified to

$$T(R_p) = T < T + \theta_0 \exp - (t/t_1)^{\frac{1}{2}}, \quad (14)$$

which explains the impossibility of an instantaneous condensation during adherence.

5.2.3. *Heat transfer to individual bubbles.* For the heat transmission to a free vapour bubble it follows from equations (29) and (16) of Part I [2], that:

(i) the rate of heat flow

$$\Phi_b = 4\pi\rho_2 l R^2 \dot{R} = 2\pi\rho_2 l C_2^3 t^{\frac{1}{2}} \cong 2\pi\rho_2 l C_1^3 (\Delta\theta_0)^3 t^{\frac{1}{2}},$$

(ii) the heat flux density

$$q_b = \rho_2 l \dot{R} = \tfrac{1}{2}\rho_2 l C_2 t^{-\frac{1}{2}} \cong \tfrac{1}{2}\rho_2 l C_1\, \Delta\theta_0 t^{-\frac{1}{2}},$$

and

(iii) the coefficient of heat transfer

$$h_b = (q_b/\Delta\theta_0) \cong \tfrac{1}{2}\rho_2 l C_1\, t^{-\frac{1}{2}}.$$

For adhering and released bubbles, these quantities can be derived now from the experimental $R(t)$-curves during the whole lifetime of a bubble. Note, that $\Phi_b \sim t^{\frac{1}{2}}$, and that both q_b and $h_b \sim t^{-\frac{1}{2}}$. Also, $\Phi_b \sim C_1^3$, and both q_b and $h_b \sim C_1$. Thus where the heat transmission to individual bubbles in 4·1 wt % methylethylketone is reduced considerably in comparison to water on account of the severe decrease in the growth constant C_1.

5.2.4. *Conclusions.* Summarizing the experimental results of the preceding Sections 4 and 5, the following ratios of the corresponding quantity in 4·1 wt % methylethylketone in comparison to water have been determined: $q_{w,\max}$: 2·7; $\Delta\theta_0$ for motion pictures: 2·7; θ_0 for motion pictures: 1·20; C_2 for released bubbles: 0·50; C_1 for released bubbles: 0·20, and average $R_1 = R(t_1)$: 0·23 by taking only bubbles with $\Delta\theta_0 = 0{\cdot}36$ degC in water.

It is seen here, that the expected coincidence, cf. Part I [2], of an increased peak flux density, a slowing down of bubble growth, and a decreased bubble departure radius, has been proved to occur experimentally. For the theoretical explanation reference is made to van Stralen's relaxation microlayer theory [12].

The growth coefficient C_1 has been shown to be only slightly dependent on the liquid superheating, in accordance with Scriven's theory, cf. Part I [2]. Released bubbles have been investigated instead of the theoretical free bubbles; the mutual distance of the bubbles was of the order of their diameter. A severe competition in the consumption rate of the more volatile component must occur between neighbouring bubbles at actual peak flux conditions, in

consequence of the corresponding high density of bubble population.

6. BUBBLE GROWTH IN WATER–1-BUTANOL MIXTURES

6.1. *Results for* 1·5 *wt* % 1-*butanol*

The field of view of the camera is shown in Fig. 15. The distribution of active sites on the heating surface in which bubbles are promoted is indicated in the caption of this figure. A superheating $\Delta\theta_0 = 0{\cdot}14$ degC (cf. Figs. 4 and 5) has been measured in the liquid near the nucleus generating the vibrating bubbles ***b***, ***c***, ***d*** and ***a*** [10].

For the successive bubbles ***b***, ***c*** and ***d*** (Fig. 16) and for bubble ***a*** (Fig. 17) the growth factor in equation (11) amounts to $C_{2,m} = 2{\cdot}5 \times 10^{-4}$ m/s$^{\frac{1}{2}}$, i.e. $C_{1,m} = C_{2,m}/\Delta\theta_0 = 18 \times 10^{-4}$ m/s$^{\frac{1}{2}}$ degC, in comparison to $C_{2,p} = 11{\cdot}5 \times 10^{-4}$ m/s$^{\frac{1}{2}}$ for released bubbles moving upwards to the liquid-level surface in water with a superheating $\Delta\theta_0 = 0{\cdot}36$ degC, cf. equation (7).

The average time of adherence to the heating wire for these bubbles is equal to $5{\cdot}3 \times 10^{-3}$ s,

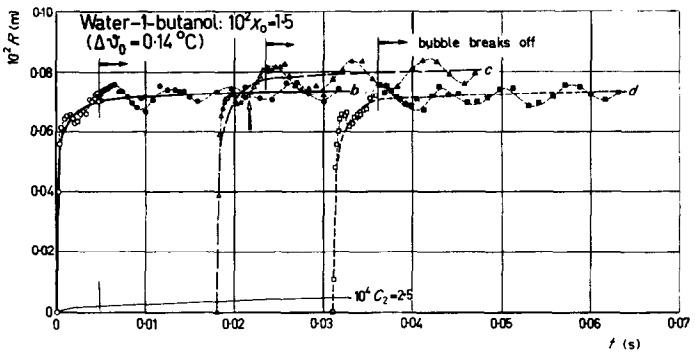

FIG. 16. 1·5 wt % 1-*butanol*. Growth of consecutive vibrating vapour bubbles, generated on the same nucleus; $\Theta_0 = 21$ degC and $\Delta\theta_0 = 0{\cdot}14$ degC.

Curve $R = 2{\cdot}5 \times 10^{-4}\, t^{\frac{1}{2}}$ denotes theoretical growth of free bubbles subjected only to the superheating of bulk liquid.

Arrow on curve for bubble ***b*** denotes the frame shown in photograph 2 of Fig. 18.

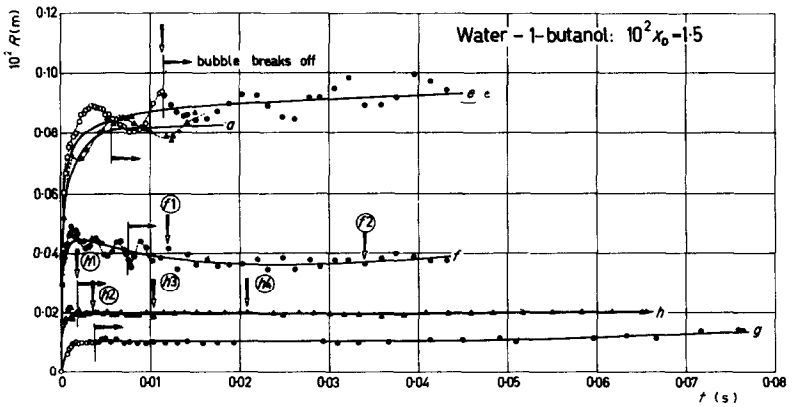

FIG. 17. 1·5 wt % 1-*butanol*. Growth curves for vapour bubbles, generated on various nuclei at the wire (cf. Fig. 15); $\theta_0 = 21$ degC.

Arrows on curves for bubbles ***e***, ***f*** and ***h*** denote the frames shown in Figs. 15, 18 and 19, respectively.

i.e. 35 per cent shorter than in water (8×10^{-3} s). A number of bubbles show an unusual growth rate after breaking away from the wire:

1. The nucleus generating bubble *e* is rather free from neighbouring active sites (cf. Fig. 15). This results in a relatively small consumption rate of the more volatile component in the liquid near this nucleus and probably also in a larger local liquid superheating in comparison to the nucleus generating bubbles *b*, *c*, *d* and *a*. Consequently, the growth rate of bubble *e* has been increased to a value corresponding with $C_{2,m} = 4 \times 10^{-4}$ m/s$^{\frac{1}{2}}$, after the instant of breaking away from the heating surface (Fig. 17).

2. The size of bubble *f* decreases gradually during the first $1{\cdot}5 \times 10^{-2}$ s after release, Fig. 17. This is due to a close proximity of this bubble to two other bubbles, one of which is growing rapidly at the heating wire, Fig. 18. Bubble *f* grows again if the distance to the next neighbours has been increased considerably (Figs. 17 and 18).

3. The small bubbles *g* and *h* are breaking away below the heating wire before rising again (Fig. 19). The growth of these bubbles is stopped completely after the initial stage because a large number of successive bubbles grows rapidly in their neighbourhood.

6.2. *Results for* 6·0 *wt* % 1-*butanol*

The field of view is shown in Fig. 20. A superheating $\Delta\theta_0 = 0{\cdot}31$ degC (cf. Figs. 4 and 5) has been measured in the liquid near the nucleus generating the bubbles studied (Figs. 21 and 22). Bubbles *b*, *c* and *e* are rather free from near neighbours during the first $3{\cdot}5 \times 10^{-2}$ s (Fig.

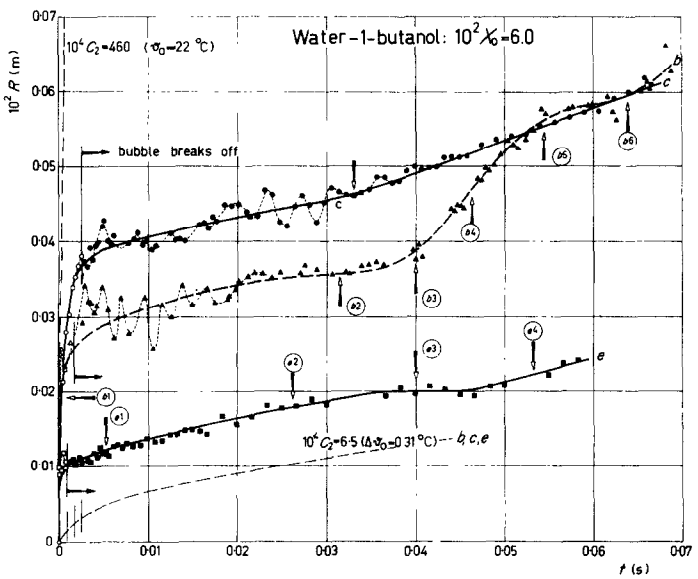

FIG. 21. 6·0 wt % 1-*butanol*. Growth of vibrating vapour bubbles. Curve $R = 6{\cdot}5 \times 10^{-4}\ t^{\frac{1}{2}}$ denotes theoretical growth of free bubbles subjected only to the superheating of bulk liquid $\Delta\theta_0 = 0{\cdot}31$ degC. Curve $R = 460 \times 10^{-4}\ t^{\frac{1}{2}}$ denotes growth of free bubbles subjected only to the wire superheating $\theta_0 = 22$ degC.

The growth of released bubbles corresponds with this curve during the first 3×10^{-2} s after departure. The deviations in growth rate at later instants result from changes in the surrounding bubble population.

Arrows on curves for bubbles *b*, *c* and *e* denote the frames, shown in Figs. 23, 20 and 24, respectively.

21). The growth factor in equation (11) for these bubbles is $C_{2,m} = 6{\cdot}5 \times 10^{-4}$ m/s$^{\frac{1}{2}}$, i.e. $C_{1,m} = C_{2,m}/\Delta\theta_0 = 21 \times 10^{-4}$ m/s$^{\frac{1}{2}}$ degC. Exceptional or unusual growth rates have been observed for

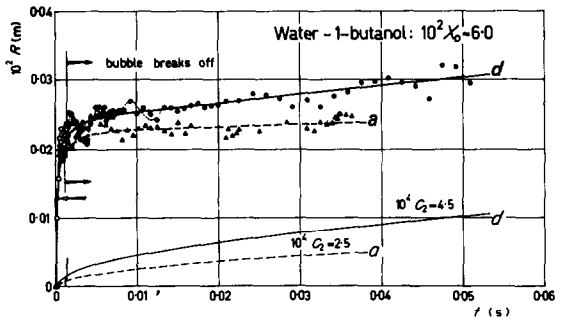

FIG. 22. 6·0 wt % 1-*butanol.* Growth of vibrating vapour bubbles; $\theta_0 = 22$ degC. Curves $R = 2{\cdot}5 \times 10^{-4}\ t^{\frac{1}{2}}$ (bubble *a*) and $R = 4{\cdot}5 \times 10^{-4}\ t^{\frac{1}{2}}$ (bubble *d*) denote theoretical growth for free bubbles. Bubbles *a* and *d* are disturbed continuously and their growth rate is slowed down due to a close proximity to neighbouring bubbles.

Arrow on curve for bubble *a* denotes the frame shown in Fig. 20.

several bubbles in this mixture too (cf. Section 5 for 4·1 wt % methylethylketone):

1. Bubble *b* (and bubble *c*) moves forward after 4×10^{-2} s, outside the range of competitive consumption of the more volatile component by neighbouring bubbles (Fig. 23). This results in an increased growth rate (Fig. 21).

2. The growth of bubble *e* is stopped during 10^{-2} s owing to its close proximity to two larger bubbles (Figs. 21 and 24).

3. The growth rate of the released bubbles *a* and *d* has been slowed down continuously as a result of a close proximity to several neighbouring bubbles (Fig. 22).

6.3. *Other observations*

Some other characteristic phenomena were also observed and may be worth reporting here:

1. The bubble radius R_1 at the instant of breaking away from the heating surface is in the mixtures considerably smaller than in water. This radius varies from 4×10^{-4} m to 11×10^{-4} m in water (cf. Section 4), from 10^{-4} m to 9×10^{-4} m in 1·5 % wt 1-butanol and from 10^{-4} m to 4×10^{-4} m in 6·0 % wt 1-butanol, cf. equation (5) and [12].

2. Generally, a decrease in bubble size causes a higher frequency of vapour formation on the generating nucleus.

3. Several bubbles oscillated about the spherical form. The most important mode of vibration is the slowest, fundamental harmonic. A sphere is transformed periodically into a rotation ellipsoid, cf. the Appendix. Higher modes of vibration have been observed sometimes [11, 12].

4. Bubble coalescence was observed only occasionally in the mixtures. Clusters of vapour bubbles occur in 6·0 % wt 6-butanol (cf. Fig. 20) which is due to the Marangoni-effect. This is in contrast to the behaviour in water, where touching bubbles merge into each other immediately.

6.4. *Conclusions*

A minimum growth rate of released vapour bubbles occurs at a low concentration of the more volatile component, i.e. at 1·5 wt % of 1-butanol, in quantitative agreement with the exact theoretical equation (71) of Part I [2], cf. Fig. 25:

$$\frac{\Delta T}{G_d} = -x_0\{K(x_0) - 1\}\left(\frac{\mathrm{d}T}{\mathrm{d}x}\right)_{x=x_0} = \frac{\Delta\theta_0 - (\rho_2 l/\rho_1 c)\,\Phi(1 - \rho_2/\rho_1, C_{2,m}/2a^{\frac{1}{2}})}{(\rho_2/\rho_1)\,\Phi(1 - \rho_2/\rho_1, C_{2,m}/2D^{\frac{1}{2}})}. \tag{15}$$

The predicted coincidence of a maximum peak flux density in nucleate boiling and a minimum bubble growth rate has been shown to occur experimentally.

The curious behaviour of bubbles with unusual growth rates has been shown to depend on the bubble population in their nearby neighbourhood and can be explained qualitatively by the theory. The strong effect of mass diffusion on the rate of bubble growth in

mixtures is obvious, especially for these bubbles. The results on the bubble growth during adherence have been discussed previously, cf.

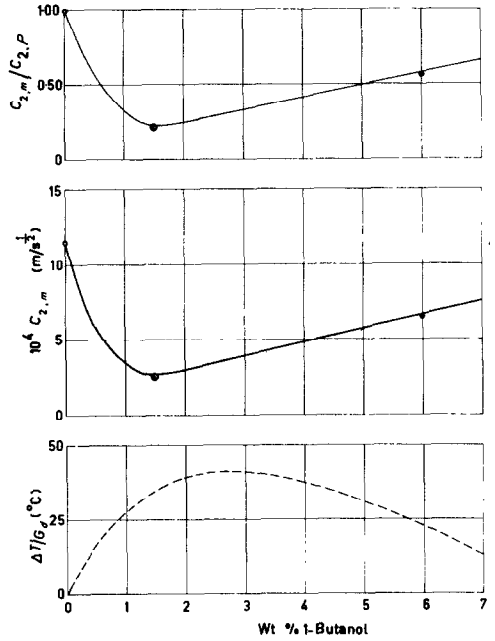

FIG. 25. *Water–1-butanol.* Experimental (○, ⊙, ●) and theoretical (curves), cf. the exact equation (15), growth factor, C_2, of bubble growth equation $R = C_2\, t^{\frac{1}{2}}$ for released vapour bubbles at the actually measured superheating of bulk liquid $\Delta\theta_0$ (0·36 degC in water, 0·14 degC in 1·5% and 0·31 degC in 6·0 wt % 1-butanol, respectively), and ratio to the corresponding value for water.

Bubble growth slows down depending on $\Delta T/G_d$, cf. equations (15) and (11). A minimum bubble growth rate is shown at 1·5 wt % 1-butanol.

The concentration of maximum $\Delta T/G_d$ exceeds the concentration of minimum $C_{2,m}$ slightly on account of the gradual decrease of the latent heat of vaporization for increasing concentration of the more volatile component, cf. equation (11).

Experimental results and theoretical predictions are in quantitative agreement.

Parts I and II of [12]. The growth constant C_1 determines both the initial and the subsequent bubble growth, and also the departure radius.

7. BUBBLE GROWTH IN THE AZEOTROPIC WATER–ETHANOL MIXTURE

This mixture contains 95·6 wt % ethanol; the atmospheric boiling point is $T = 351{\cdot}2°K$. The composition of vapour and liquid are the same, i.e. $y = x$, whence $\Delta T = 0$; the mixture behaves like a pure component, and is suitable for giving information about pure ethanol.

The theoretical growth factor $C_{2,p}$ (cf. Fig. 5 of Part I [2]) is shown in Fig. 26 in dependence on liquid superheatings up to 1·25 deg C.

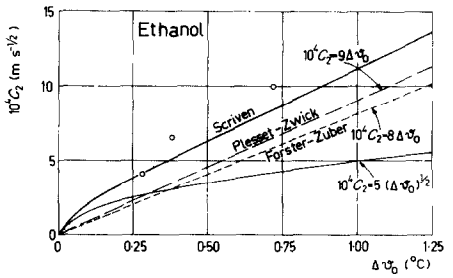

FIG. 26. 95·6 wt % *ethanol.* Theoretical growth coefficient C_2 of equation $R = C_2\, t^{\frac{1}{2}}$ for vapour bubbles as a function of liquid superheating. The straight line $C_2 = 9 \times 10^{-4}\ \Delta\theta_0$ was predicted by Plesset and Zwick and is similar to Scriven's approximation for large superheatings. The initial part of Scriven's curve can be approximated by the parabola $C_2 = 5 \times 10^{-4}\ (\Delta\theta_0)^{\frac{1}{2}}$. Experimental values are given by ○, cf. Figs. 28 and 29.

A motion picture was taken at a speed of 3000 f.p.s. [11] and illustrates bubble formation and growth both in nucleate boiling and in film boiling. The azeotropic water–ethanol mixture has been studied on account of the relatively low peak flux density in nucleate boiling, through which the possibility of burnout of the heating wire is diminished considerably in comparison with water.

7.1. *Liquid superheating in nucleate boiling and in film boiling*

The superheating of bulk liquid $\Delta\theta_0$ has been shown in Fig. 27 (left) as a function of the power of the electrical bottom heater. $\Delta\theta_0 = 0{\cdot}28$ degC at $\Theta_0 = 25$ degC and $\Delta\theta_0 = 0{\cdot}38$ degC at $\Theta_0 = 30$ degC for vapour bubbles *a* and *b*, respectively, generated in the region of nucleate boiling (Fig. 28); $\Delta\theta_0 = 0{\cdot}72$ degC at $\Theta_0 = 290$ degC for bubble *c* investigated in the region of film boiling (Fig. 29). The superheating $\Delta\theta_0$ was

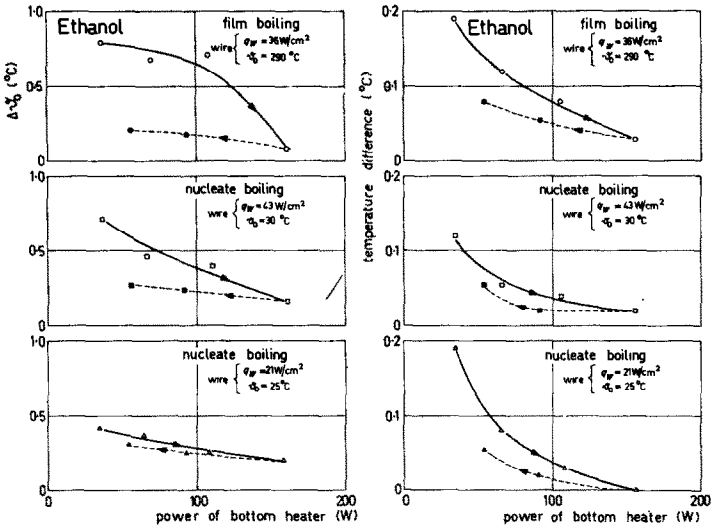

FIG. 27. 95·6 wt % *ethanol. Left*: Superheating $\Delta\theta_0$ of bulk liquid as a function of the power of the bottom heater for increasing (———) and for decreasing (– – – –) power. The same platinum wire has been used in various runs. The boiling vessel was provided with bubble screen and ground glass. The motion pictures were taken at gradually increasing temperature of the wire and at constant power of bottom heater of heater of 100 W; the superheatings of the curves for increasing power are representative in this case. *Right*: see text.

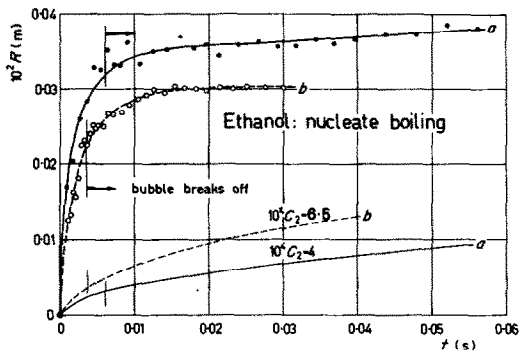

FIG. 28. 95·6 wt % *ethanol.* Growth curves for vapour bubbles generated in nucleate boiling.

The parabolas $R = 4 \times 10^{-4}\, t^{\frac{1}{2}}$ and $R = 6{\cdot}5 \times 10^{-4}\, t^{\frac{1}{2}}$ denote growth of free bubbles, subjected only to the superheating of bulk liquid $\Delta\theta_0 = 0{\cdot}28$ degC (bubble *a*) and $\Delta\theta_0 = 0{\cdot}16$ degC (bubble *b*).

measured at the point (A), 3 mm above the centre of the platinum wire.

It is reported, that

(i) The drawings on the right of Fig. 27 give the temperature difference between point (A) and point (B); point (B) is located on the parallel line, 3 mm above the same wire, and at a distance of 1·6 cm from the centre, i.e.

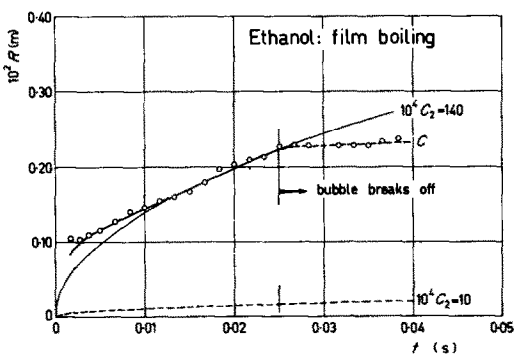

FIG. 29. 95·6 wt % *ethanol.* Growth curve for a vapour bubble generated at the vapour–liquid interface of the vapour film surrounding the wire in film boiling.

Growth during adherence can be approximated by $R = 140 \times 10^{-4}\, t^{\frac{1}{2}}$, growth after departure by $R = 10 \times 10^{-4}\, t^{\frac{1}{2}}$, cf. the parabola at the bottom.

The (large) bubble radius at the instant of breaking away from the interface is approximately 7 times the value for bubble *a* of Fig. 28, the ratio of the times of adherence is 4.

close to the end of the wire. The local superheating of the liquid at point (B) is slightly lower than at point (A)—cf. Fig. 1 for water—i.e. at a power of the bottom heater of 100 W, $\Delta\theta_0$(B) = 0·28–0·04 = 0·24 degC for θ_0 = 25 degC, $\Delta\theta_0$(B) = 0·38–0·04 = 0·34 degC for θ_0 = 30 degC, and $\Delta\theta_0$(B) = 0·72–0·08 = 0·64 degC for θ_0 = 290 degC in film boiling.

(ii) Drawings on the *left* and on the *right*: The The hysteresis effect in the curves $\Delta\theta_0$ vs. power of heater, which has been measured both at points (A) and (B), is probably due to the nucleation of active sites, cf. also Fig. 1 of Part I [2]. Once the nuclei are activated at a higher temperature of the bottom plate, they remain active as the temperature decreases, at least for some time, cf. Part III of [12]. This results in lower values of $\Delta\theta_0$.

7.2. *Nucleate boiling*

The experimental value for the growth factor is $C_2 = 4 \times 10^{-4}$ m/s$^{\frac{1}{2}}$ at $\Delta\theta_0$ = 0·28 degC (Fig. 28, bubble *a*), and $C_2 = 6{\cdot}5 \times 10^{-4}$ m/s$^{\frac{1}{2}}$ at $\Delta\theta_0$ = 0·38 degC (Fig. 28, bubble *b*). The first value is in agreement with Scriven's theoretical value (cf. Fig. 26), the latter is 30 per cent higher. Scriven's values, which are obtained by taking into account the effect of radial convection on bubble growth, cf. Part I [2], are in better agreement with the experimental results than Forster and Zuber's and Plesset and Zwick's predictions. This result is similar to the case of water, cf. Section 4.

7.3. *Film boiling*

The growth of a (large) vapour bubble, generated at and released from the vapour–liquid interface of the vapour film surrounding the heating wire in the region of film boiling, is shown in Fig. 29. The growth factor $C_2 = 10 \times 10^{-4}$ m/s$^{\frac{1}{2}}$ at $\Delta\theta_0$ = 0·72 degC after release, in reasonably good agreement with Scriven's theoretical value $C_2 = 8{\cdot}5 \times 10^{-4}$ m/s$^{\frac{1}{2}}$ at the same $\Delta\theta_0$, cf. Fig. 26. It is striking, that the entire growth curve during adherence can be approximated by $C_2 = 140 \times 10^{-4}$ m/s$^{\frac{1}{2}}$, which corresponds according to Plesset and Zwick's approximation $C_2 = 9 \times 10^{-4}\,\Delta\theta_0$, i.e. $C_1 = 9 \times 10^{-4}$ m/s$^{\frac{1}{2}}$ degC—with an effective liquid superheating of 16 degC. This behaviour is analogous to a time-independent value of the superheating of the relaxation microlayer, in contradiction to the exponential decrease in case of nucleate boiling, cf. equation (4) and Parts I and II of [12]. Similar bubble growth curves have been observed by Cole and Shulman [22, 23], nevertheless not in film boiling, but in nucleate boiling.

7.4. *Conclusions*

The theoretical predictions for free vapour bubbles, generated in nucleate boiling of water and the azeotropic water–ethanol mixture, are shown to be in good agreement with experimental data on released bubbles. A vapour bubble generated in film boiling of the azeotropic water–ethanol mixture, grows during adherence like a free bubble in an initially uniformly superheated liquid.

REFERENCES

1. M. JAKOB, Heat transfer in evaporation and condensation, *Mech. Engng* **58**, 643–660, 729–739 (1936); *Heat Transfer*, Vol. 1. Wiley, New York (1950); W. FRITZ and W. ENDE, Über den Verdampfungsvorgang nach kinomatographischen Aufnahmen an Dampfblasen, *Phys. Z.* **37**, 391–401 (1936).
2. S. J. D. VAN STRALEN, The growth rate of vapour bubbles in superheated pure liquids and binary mixtures, Part I, *Int. J. Heat Mass Transfer* **11**, 1467–1489 (1968).
3. P. J. DERGARABEDIAN, The rate of growth of vapour bubbles in superheated water, *J. Appl. Mech.* **20**, 537–545 (1963).
4. J. W. WESTWATER and J. G. SANTANGELO, Photographic study of boiling (High speed motion picture), *Ind. Engng Chem.* **47**, 1605–1610 (1955).
5. J. W. WESTWATER, Boiling of liquids, *Adv. Chem. Engng*, **1**, 1–76 (1956); **2**, 1–31 (1958).
6. J. W. WESTWATER, Boiling Heat Transfer, *Am. Scient.* **47**, 427–446 (1959).
7. J. E. BENJAMIN and J. W. WESTWATER, Bubble growth in nucleate boiling of a binary mixture, International Heat Transfer Conference, Boulder, Colorado (1961).
8. S. J. D. VAN STRALEN, Heat transfer to boiling binary liquid mixtures at atmospheric and subatmospheric pressures, *Chem. Engng Sci.* **5**, 290–296 (1956).
9. W. R. VAN WIJK and S. J. D. VAN STRALEN, Growth

rate of vapour bubbles in water and in a binary mixture boiling at atmospheric pressure, *Physica, 's Grav.* **28**, 150–171 (1962); Maximale Wärmeströmdichte und Wachstumsgeschwindigkeit von Dampfblasen in siedenden Zweistoffgemischen, *Chemie-Ingr-Tech.* **37**, 509–517 (1965).
10. S. J. D. VAN STRALEN, Growth rate of vapour bubbles in water–1-butanol mixtures boiling at atmospheric pressure, *Physica, 's Grav.* **29**, 602–616 (1963); *Sixth International Congress on High-Speed Photography* 1962, pp. 534–539, Scheveningen, Netherlands; Tjeenk Willink, Haarlem, Netherlands (1963); Bubble growth rates in boiling binary mixtures, *Br. Chem. Engng* **12**, 390–394 [143–147] (1967).
11. S. J. D. VAN STRALEN, High speed motion picture, Agric. Univ., Wageningen, Netherlands (1960).
12. S. J. D. VAN STRALEN, The mechanism of nucleate boiling in pure liquids and in binary mixtures, Part I–IV, *Int. J. Heat Mass Transfer* **9**, 995–1020, 1021–1046 (1966); **10**, 1469–1484, 1485–1498 (1967).
13. J. M. YATABE and J. W. WESTWATER, Bubble growth rates for ethanol–water and ethanol–isopropanol mixtures, *Chem. Engng Prog. Symp. Ser.* **64**, **62**, 17–23 (1966).
14. R. SÉMÉRIA, An experimental study of the characteristics of vapour bubbles, Symposium on two-phase fluid flow, Instn Mech. Engrs, Paper No. 7 (1962).
15. W. WANNINGER, Über die Dynamik von Dampfblasen in Propan, Doctor thesis, Technische Hochschule, Stuttgart, Germany (1964); Dynamik von Dampfblasen in Propan, *Chemie-Ingr-Tech.* **37**, 939–943 (1965).
16. F. C. GUNTHER, Photographic study of surface boiling heat transfer to water with forced convection, *Trans. Am. Soc. Mech. Engrs* **73**, 115–123 (1951).
17. M. E. ELLION, A study of the mechanism of boiling heat transfer, California Inst. Technol., Jet Propulsion Lab. Mem. 20–88 (1954).
18. H. A. C. THIJSSEN, Effect of liquid composition on plate efficiency in the rectification of binary mixtures, Doctor thesis, Agric. Univ. Wageningen, Netherlands; Staatsdrukkerij, Netherlands (1955). In Dutch with English summary and captions.
19. S. J. D. VAN STRALEN, Heat transfer to boiling binary liquid mixtures, Doctor thesis, Univ. of Groningen, Netherlands; Veenman, Wageningen, Netherlands (1959); *Meded. LandbHoogesch. Wageningen* **59** (6), 1–82 (1959); In Dutch with English summary and captions; Heat transfer to boiling binary liquid mixtures, *Br. Chem. Engng* **4**, 8–17 (1959); **4**, 78–82 (1959); **6**, 834–840 (1961); **7**, 90–97 (1962).
20. W. SIEMES, Gasblasen in Flüssigkeiten, Teil II: Der Aufstieg von Gasblasen in Flüssigkeiten, *Chemie-Ingr-Tech.* **26**, 614–630 (1954).
21. C. E. FANEUFF, E. A. MCLEAN and V. E. SCHERRER, Some aspects of surface boiling, *J. Appl. Phys.* **29**, 80–84 (1958).
22. R. COLE and H. L. SCHULMAN, Bubble growth rates at high Jakob numbers, *Int. J. Heat Mass Transfer* **9**, 1377–1390 (1966).
23. S. J. D. VAN STRALEN, Comments on the paper "Bubble growth rates of high Jakob numbers", *Int. J. Heat Mass Transfer* **10**, 1908–1912 (1967).
24. LORD RAYLEIGH, *The Theory of Sound*, 2nd edn., Vols. 1, 2, Dover, New York (1945).
25. H. LAMB, *Hydrodynamics*, 6th edn. Cambridge University Press, Cambridge (1957).

APPENDIX

1. *Bubble Oscillations*

According to Rayleigh [24] for liquid drops and to Lamb [25] both for drops and bubbles, the angular frequency of undamped, free bubble oscillations is given by:

$$\omega_0^2 = \left(\frac{2\pi}{\tau_0}\right)^2 = (m+1)(m-1)(m+2)\frac{\sigma}{\rho_1 R^3}. \tag{16}$$

In the most important mode of vibration, the slowest fundamental harmonic, a sphere is transformed periodically into a rotation ellipsoid with $a_1 > a_2$ and $a_1 < a_2$, respectively. One has $m = 2$ in this case, whence

$$\omega_0^2 = 12\frac{\sigma}{\rho_1 R^3}. \tag{17}$$

The oscillations are due to a periodical exchange of free energy or potential energy of capillarity (which is maximal in the position of maximal deviation from a sphere) and kinetic energy (which is maximal by passing the spherical shape). Equation (16) has been derived by assuming a constant bubble volume V. The angular frequency of the corresponding damped oscillations (underdamped case) follows from:

$$\omega^2 = \omega_0^2 - f^2, \tag{18}$$

where the viscous damping coefficient can be calculated from the following theoretical expression, which yields for $m = 2$:

$$f = (m+2)(2m+1)\frac{\eta}{\rho_1 R^2} = 20\frac{\eta}{\rho_1 R^2} = 20\frac{\nu}{R_1^2}. \tag{19}$$

This coefficient can also be derived from the gradually decreasing amplitude:

$$A(t) = A(0)\exp(-ft). \tag{20}$$

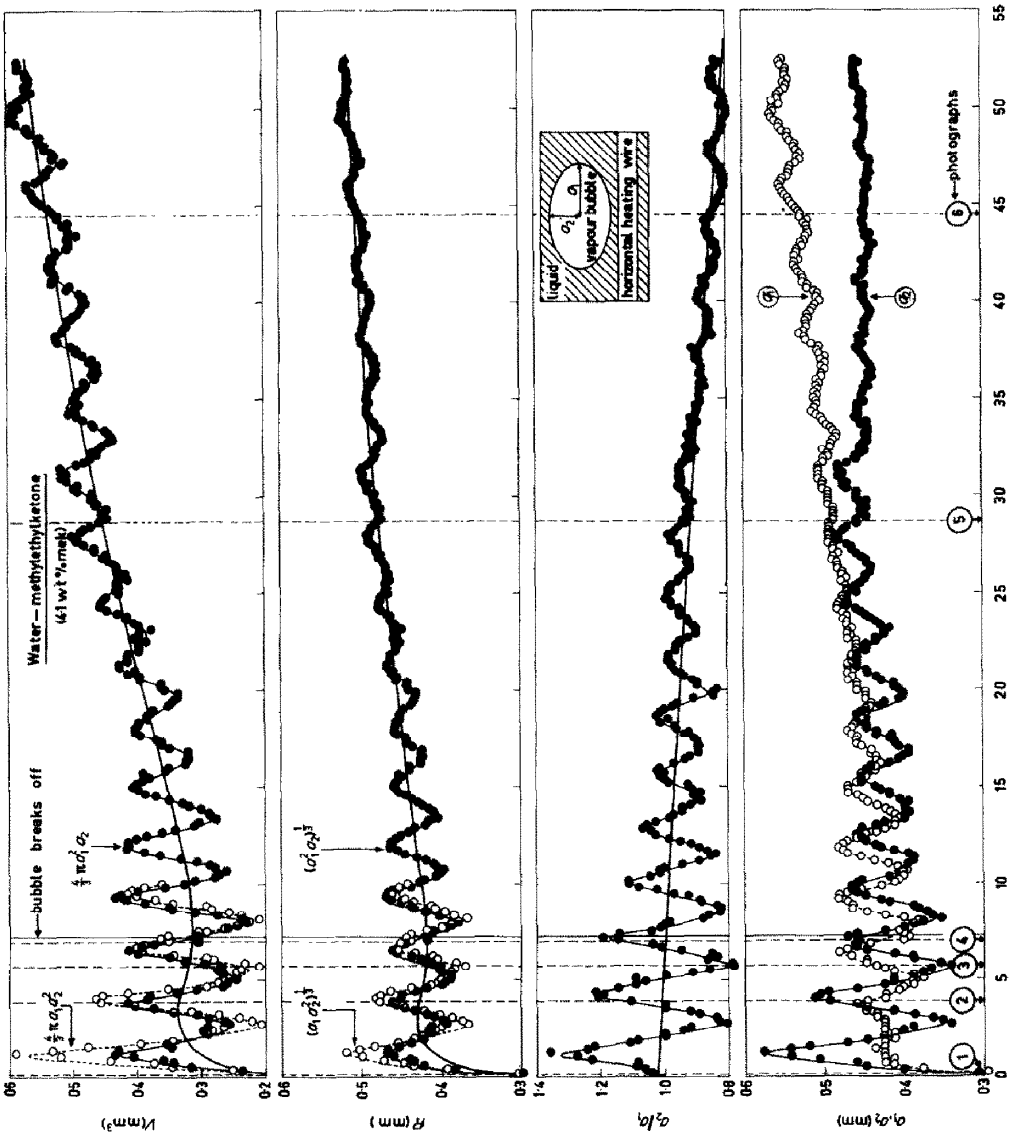

FIG. 30. 4·1 wt % *methylethylketone*. Growth and vibrations of bubble *a* of Fig. 11. Referred to in the photographs in Fig. 12.

Table 1. 4·1 wt % *methylethylketone. Data for bubble a of Figs.* 11–13 *and* 30. *The kinematic viscosity* $\nu = 3{\cdot}3 \times 10^{-7}$ m^2/s *and the surface tension constant* $\sigma = 0{\cdot}0414$ kg/s^2 *at the atmospheric boiling point* $T = 362$°K. *Values have been calculated for* $R_{1,m} = 4{\cdot}2 \times 10^{-4}$ m

$10^{-3}\,\omega_0$ (1/s)	$10^{3}\,\tau_0$ (s)	$10^{-3}\,\omega$ (1/s)	$10^{3}\,\tau$ (s)	viscous damping coefficient f (1/s)		
theoretical equation (16)		experimental Fig. 30, at $t = t_{1,m}$		experimental equation (20)	equation (18)	theoretical equation (19)
2·56	2·45	2·33	2·70	52	34	37

Bubble *a* in 4·1 wt % methylethylketone (cf. Figs. 11, 12 and 13) shows only the oscillation with $m = 2$, though several other bubbles in water and mixtures vibrate also in higher modes, cf. e.g. Fig. 4 of Part I of [12]. The bubble radius depends on time here; one has, after departure:

$$R_m(t) = R_{1,m} = C_{1,m}\,\Delta\theta_0(t^{\frac{1}{2}} - t_{1,m}^{\frac{1}{2}}), \quad (21)$$

whence $R_m(t)$ increases, and $\omega_0 \sim R_m^{-\frac{1}{2}}$ decreases gradually (Fig. 30). We consider here the behaviour for $R_{1,m} = R(t_{1,m}) = 4{\cdot}20 \times 10^{-4}$ m.

Experimental data and calculated values for this bubble are given in Fig. 30 and Table 1. It follows from Table 1, that the agreement between theoretical and experimental values is good.

It may be worth reporting here, that numerical values of σ and η (practically at arbitrary temperature by varying the pressure) can be obtained by studying vibrations of vapour bubbles in boiling liquids.

It is striking, that the bubble volume is varying during vibrations of the bubble investigated (Fig. 30): V oscillates within ± 30 per cent and R oscillates within ± 10 per cent during the initial 10^{-2} s.

One has by considering the horizontal main axis as rotation symmetric, instead of the vertical main axis, cf. equation (2), that $R = (a_1 a_2^2)^{\frac{1}{3}} \approx (1/3)\,(a_1 + 2a_2)$, cf. [23]. In the latter case, the amplitude of the vibrations even increases relatively (Fig. 30). It is thus very likely, that the oscillations in volume exist actually. The cause of these oscillations, which occur without a previous bubble coalescence, is not known at present, cf. also [6]. Roughly speaking, the oscillations of V and a_2 are in phase, i.e. the bubble volume is maximal as the ratio of the semi-axes a_2/a_1 is maximal (cf. Fig. 30 with Fig. 12).

Some photographs of bubble oscillations due to coalescence have been published previously, cf. Figs. 4 and 5 of Part III of [12].

2. *Flattening of Ascending Bubbles*

A relatively small ascending bubble is flattened in first approximation to a rotation ellipsoid according to Siemes [20]. This flattening follows from the well-known Bernoulli equation. Apparently, a_2 is the rotation axis, in agreement with equation (2). In Fig. 30, a linear decrease of the ratio a_2/a_1 is shown from an initial value of 1·00 (sphere) to 0·80 after 5×10^{-2} s. After 3×10^{-2} s, a_2 is independent of time and the bubble grows then only on account of a gradual increase in a_1.

Résumé—On a étudié les vitesses de croissance des bulles, engendrées pour une densité de flux de chaleur modérée en ébullition nucléée sur un fil de platine chauffé électriquement et immergé dans l'eau, dans les mélanges eau–méthyl éthylcétone ($x_0 = 4{,}1 \times 10^{-2}$) et eau–1-butanol ($x_0 = 1{,}5 \times 10^{-2}$ et $x_0 = 6{,}0 \times 10^{-2}$). On a employé au point de vue technique une caméra à grande vitesse. Les valeurs expérimentales des constantes de croissance, $C_{1,p}$ et $C_{1,m}$ pour les bulles libérées vers le haut sont généralement en accord quantitatif avec les prévisions théoriques pour les bulles libres, par exemple, l'existence d'un $C_{1,m}$ minimal pour $x_0 = 1{,}5 \times 10^{-2}$ avec le mélange eau–1-butanol. Pour le mélange eau–méthyléthylcétone, $C_{1,m} = 0{,}20\,C_{1,p}$ et $R_{1,m} = 0{,}35\,R_{1,p}$ diminuent.

Cependant, plusieurs bulles montrent un comportement inhabituel, c'est-à-dire des vitesses de croissance plus élevées ou plus faibles provenant respectivement de l'augmentation ou de la diminution de la distance

aux bulles les plus proches. Quelquefois, on a observé des bulles qui oscillent à la fois en forme et en volume. Dans la plupart des cas, ces vibrations ne proviennent pas de la coalescence. L'amplitude des oscillations diminue à cause de l'amortissement visqueux et les bulles montantes s'aplatissent graduellement.

La fréquence du mode de vibration le plus important, c'est-à-dire le fondamental le plus lent, est en accord avec la théorie.

Quelques bulles, engendrées dans l'ébullition nucléée et dans l'ébullition par film du mélange azéotropique eau–éthanol, ont été étudiées. Un effet d'hystérésis dans la surchauffe liquide locale a été observé.

Zusammenfassung—Es wurden die Wachstumsgeschwindigkeiten von Blasen untersucht, die durch Blasensieden an einem elektrisch beheizten, in Wasser, Wasser–Methyläthylketon ($x_0 = 4{,}1 \times 10^{-2}$) und Wasser–1-Butanol- ($x_0 = 1{,}5 \times 10^{-2}$ und $x_0 = 6{,}0 \times 10^{-2}$)-Gemischen eingetauchten Platindraht bei mässiger Wärmestromdichte erzeugt wurden. Eine Hochgeschwindigkeitskamera wurde benutzt. Die experimentellen Werte der Wachstumskonstanten $C_{1,p}$ und $C_{1,m}$ für die aufsteigenden, abgelösten Blasen befinden sich im allgemeinen in guter quantitativer Übereinstimmung mit den theoretischen Voraussagen für freie Blasen, z.B. das Auftreten eines minimalen $C_{1,m}$ bei $x_0 = 1{,}5 \times 10^{-2}$ für Wasser–1-Butanol. Für das untersuchte Wasser–Methyläthylketon-Gemisch tritt ein vermindertes $C_{1,m} = 0{,}20\ C_{1,p}$ und ein vermindertes $R_{1,m} = 0{,}35\ R_{1,p}$ auf.

Zahlreiche Blasen zeigen jedoch ein ungewöhnliches Verhalten, d.h. je nach einem vergrösserten oder verkleinerten Abstand von den nächstgelegenen Nachbarblasen, höhere oder niedrigere Wachstumsraten. Manchmal wurden Blasen beobachtet, deren Kontur und Volumen oszillierten. In den meisten Fällen stammen diese Schwingungen nicht von einem Zusammenwachsen der Blasen. Die Amplitude der Schwingungen nimmt wegen der viskosen Dämpfung ab und die aufsteigenden Blasen werden allmählich abgeflacht.

Die Frequenz der wichtigsten Schwingungsart, der harmonischen Grundschwingung, stimmt mit der Theorie überein.

Einige Blasen, die bei Blasen- und Filmsieden des azeotropen Wasser–Äthanol-Gemisches erzeugt wurden, sind untersucht worden. Dabei wurde ein Hysterese-Effekt bei örtlicher Flüssigkeits-Überhitzung beobachtet.

Аннотация—Исследованы скорости роста пузырьков при пузырьковом кипении с умеренной плотностью теплового потока на платиновой проволоке, нагреваемой электрическим током и погруженной в воду и смеси вода–метилэтилкетон ($x_0 = 4{,}1 \times 10^{-2}$) и вода–1-бутанол ($x_0 = 1{,}5 \times 10^{-2}$ и $x_0 = 6{,}0 \times 10^{-2}$). Наблюдения проводились с помощью высокоскоростной киносъемки. Экспериментальные значения постоянных роста $C_{1,p}$ и $C_{1,m}$ для поднимающихся оторвавшихся пузырьков, в общем, находятся в хорошем количественном соответствии с теоретическими расчетами для свободных пузырьков, например, отмечается наличие минимума $C_{1,m}$ при $x_0 = 1{,}5 \times 10^{-2}$ для смеси вода–1-бутанол. Для смеси вода–метилэтилкетон найдены меньшие значения $C_{1,m} = 0{,}20\ C_{1,p}$ и уменьшенное значение $R_{1,m} = 0{,}35$.

Однако поведение некоторых пузырьков отклонялось от нормы, т.е. наблюдалось увеличение или снижение скоростей роста при соответствующем увеличении или уменьшении расстояния между соседними пузырями. Иногда наблюдались пузырьки с переменной формой и объемом. В большинстве слуаев эти пульсации не были вызваны слиянием пузырьков. Амплитуда пульсации уменьшалась из-за вязкого торможения, и поднимающиеся пузырьки становились более плоскими. Частота, найденная для самой низкой основной гармоники находится в соответствии с теорией.

Исследовались некоторые пузырьки, образующиеся при пузырьковом и пленочном кипении азеотропной смеси вода–этанол. Наблюдался эффект гистерезиса при локальном перегреве жидкости.